Synchrotron for medical and public health research

Cell and tissue research with synchrotron Infrared

Dr. Sukanya Chaipayang
Sukanya@slri.or.th

Synchrotron Light Research Institute (Organization)

SR Infrared micro-spectroscopy

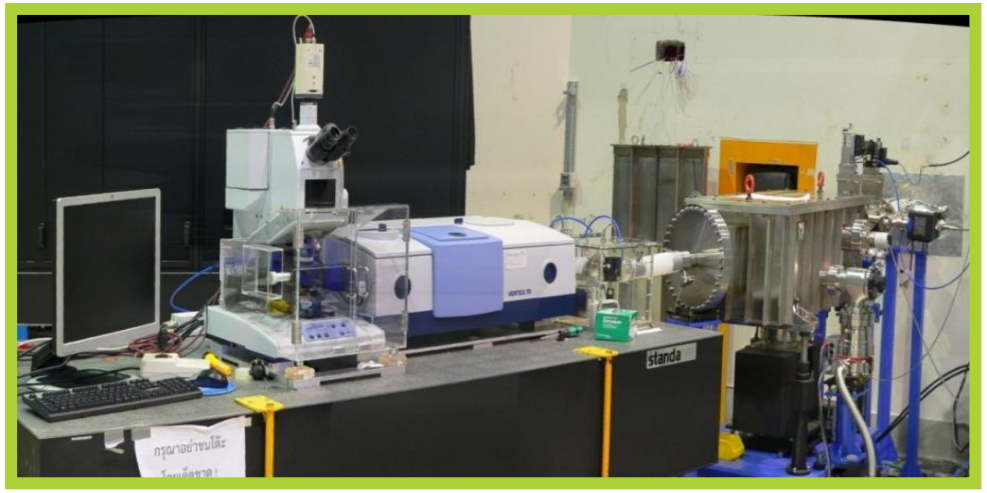

IR

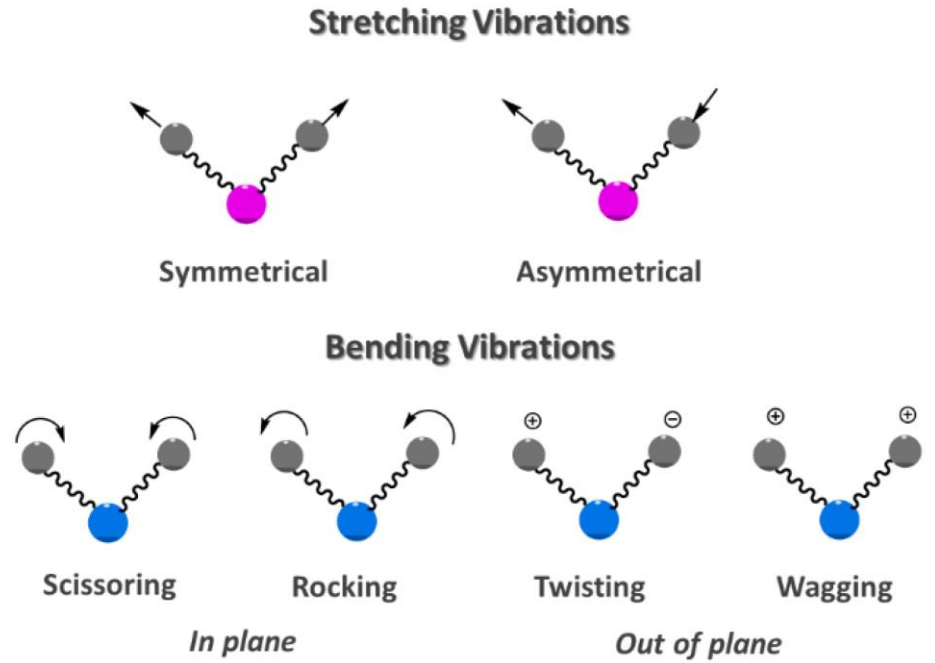

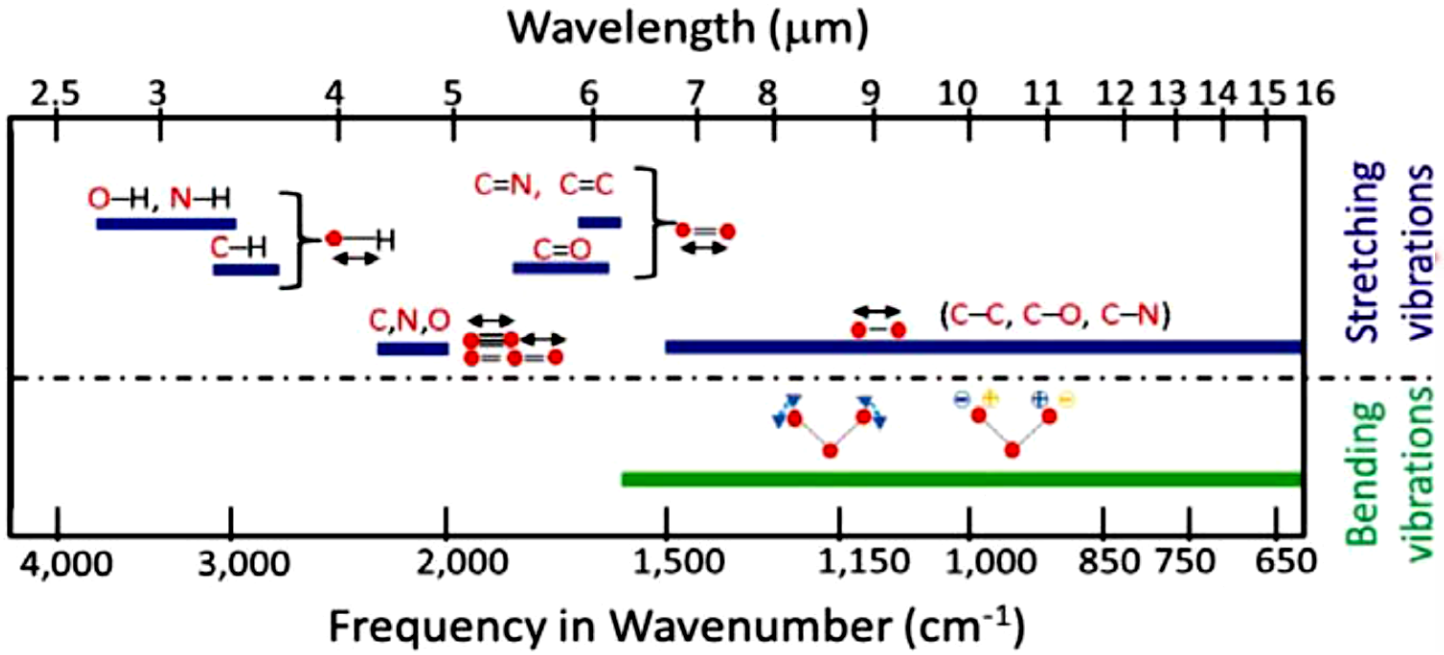

Mode of Vibration

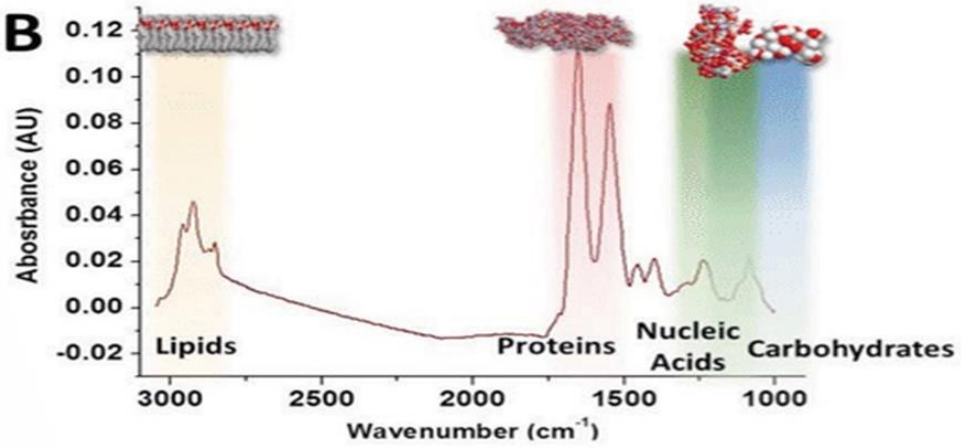

FT-IR spectrum is a fingerprint of the cells and Tissues

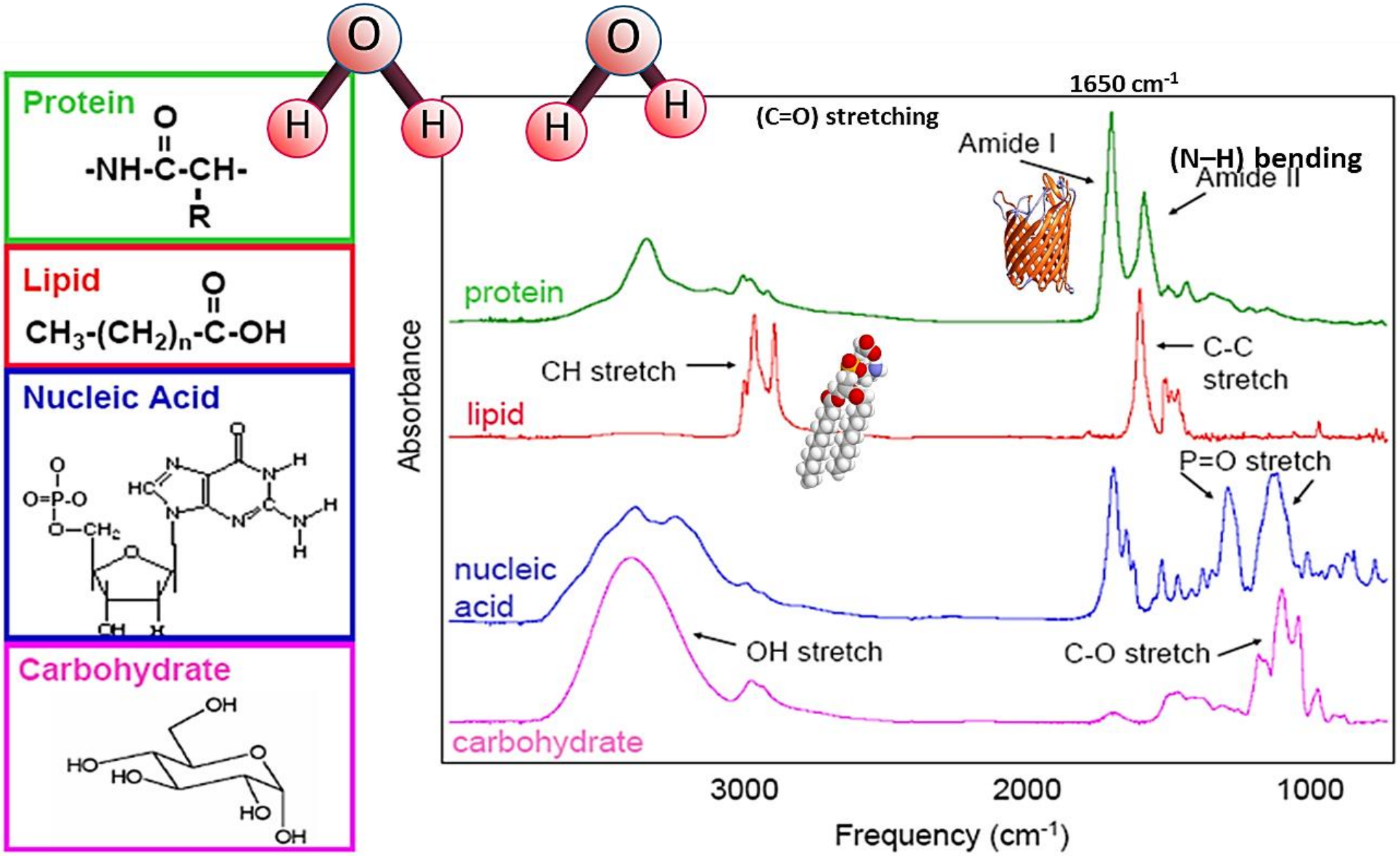

Synchrotron radiation FTIR imaging in minutes: a first step towards real-time cell imaging

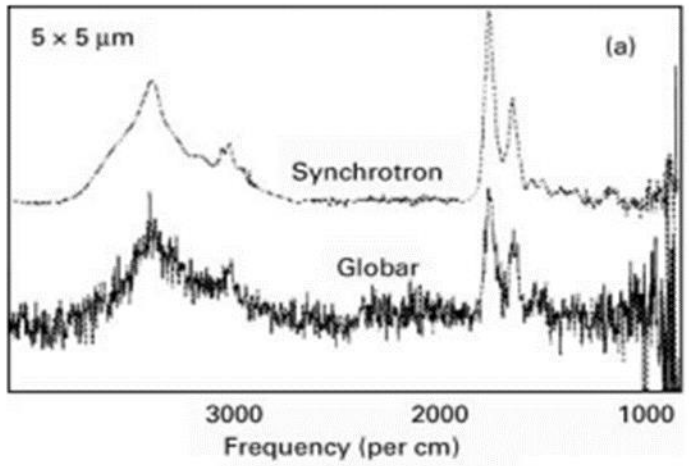

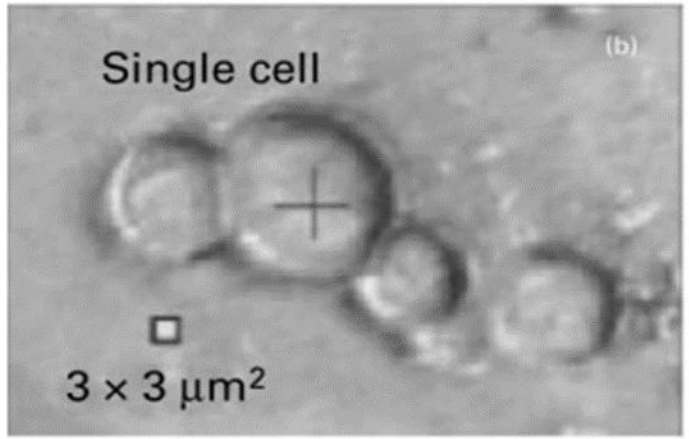

P. Yu, 2004

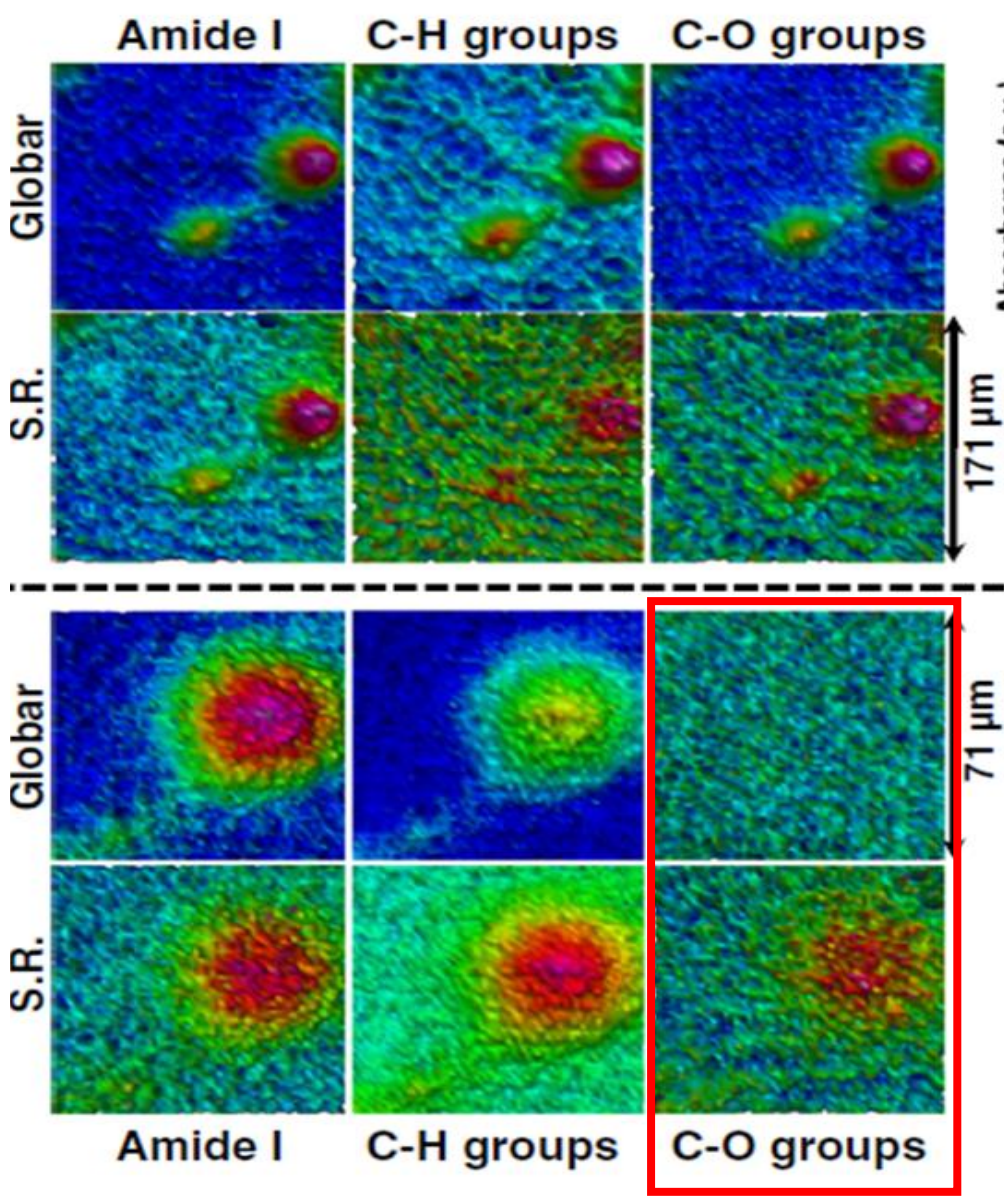

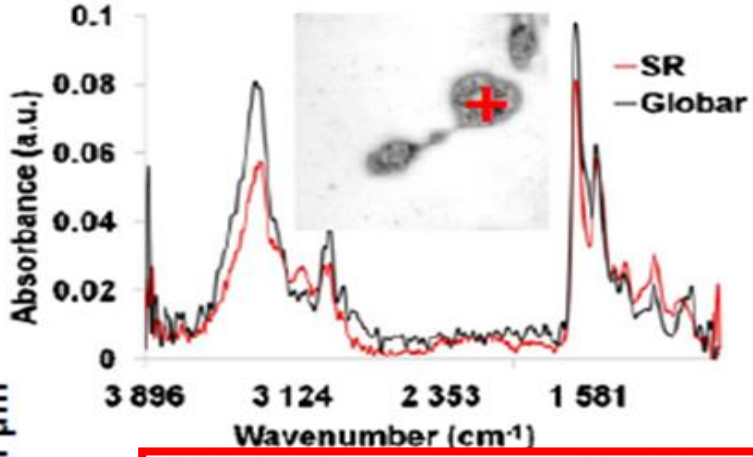

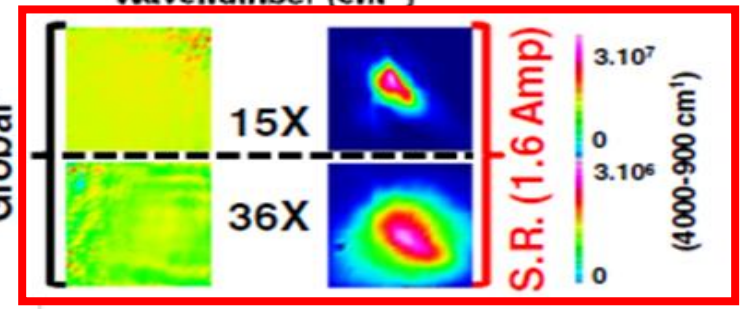

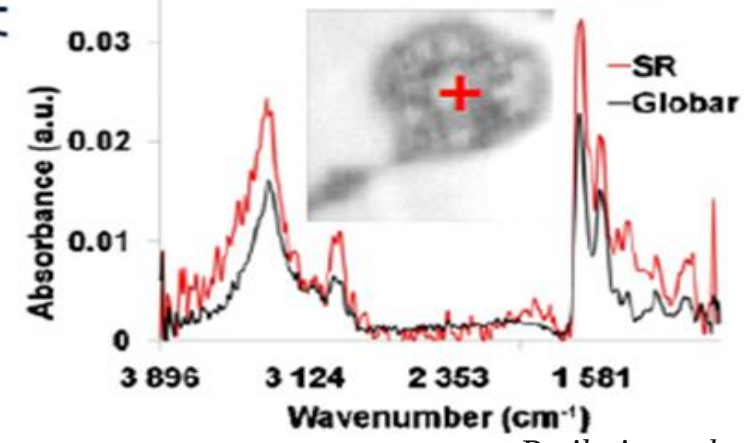

Petibois et al., 2010

Single-Cell Infrared Microspectroscopy Quantifies Dynamic Heterogeneity of Mesenchymal Stem Cells during Adipogenic Differentiation

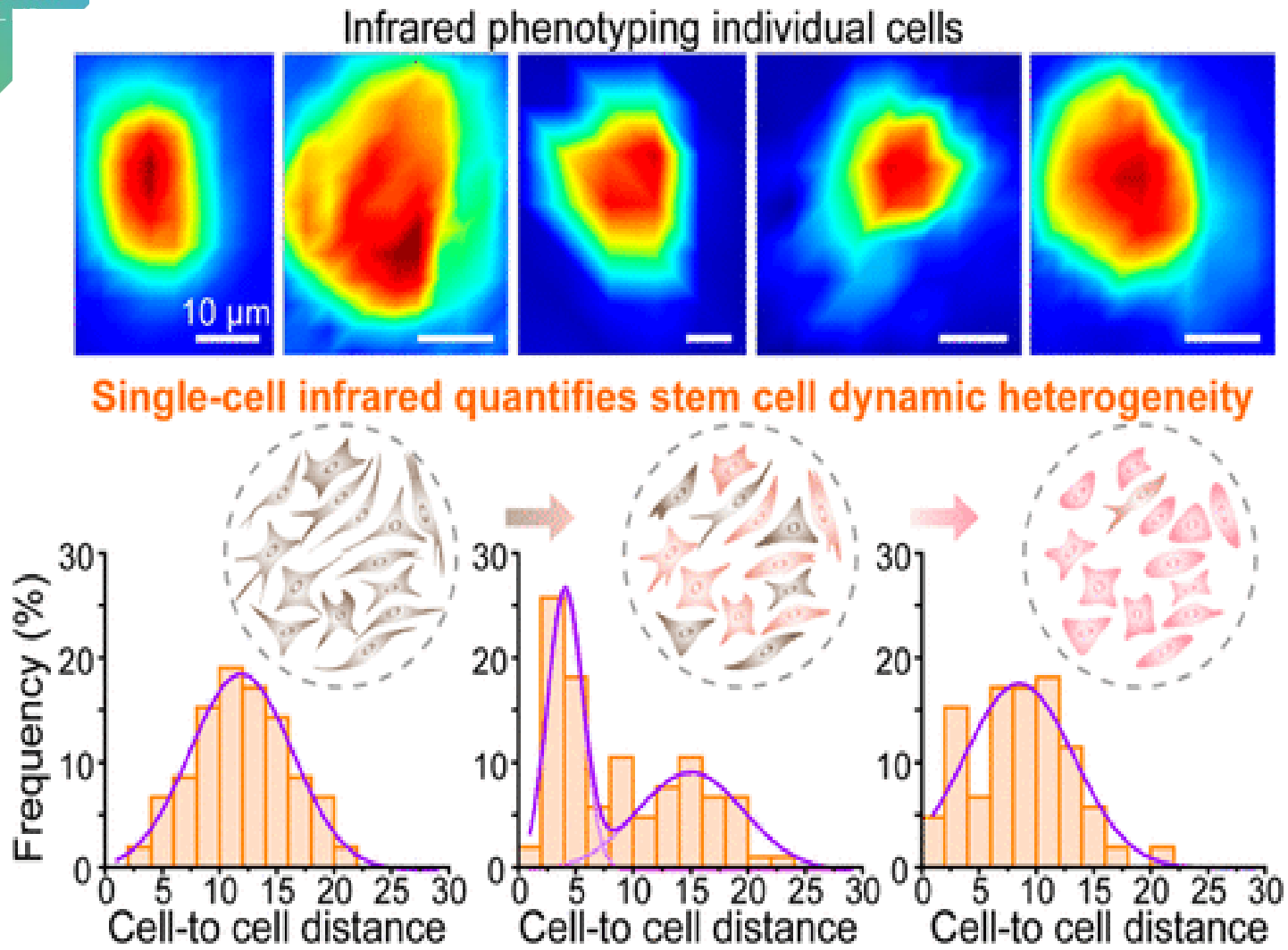

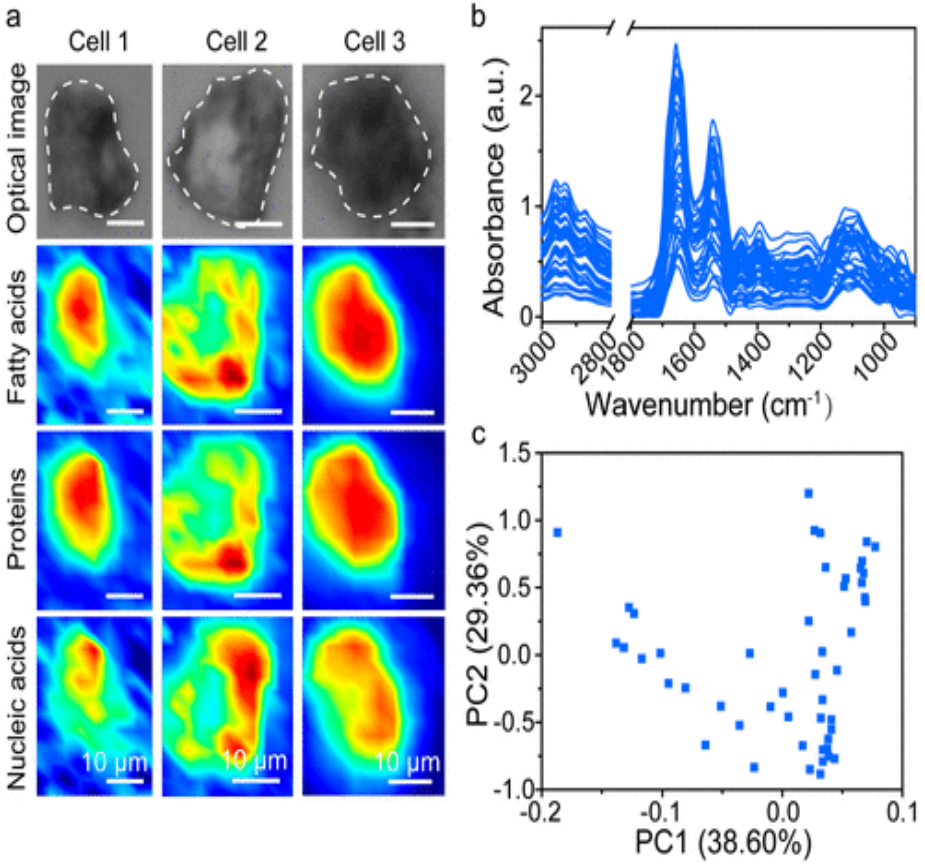

Wang et., al, 2021

Fourier-Transform Infrared Imaging Spectroscopy and Laser Ablation -ICPMS
New Vistas for Biochemical Analyses of Ischemic Stroke in Rat Brain

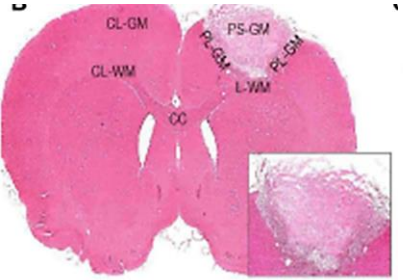

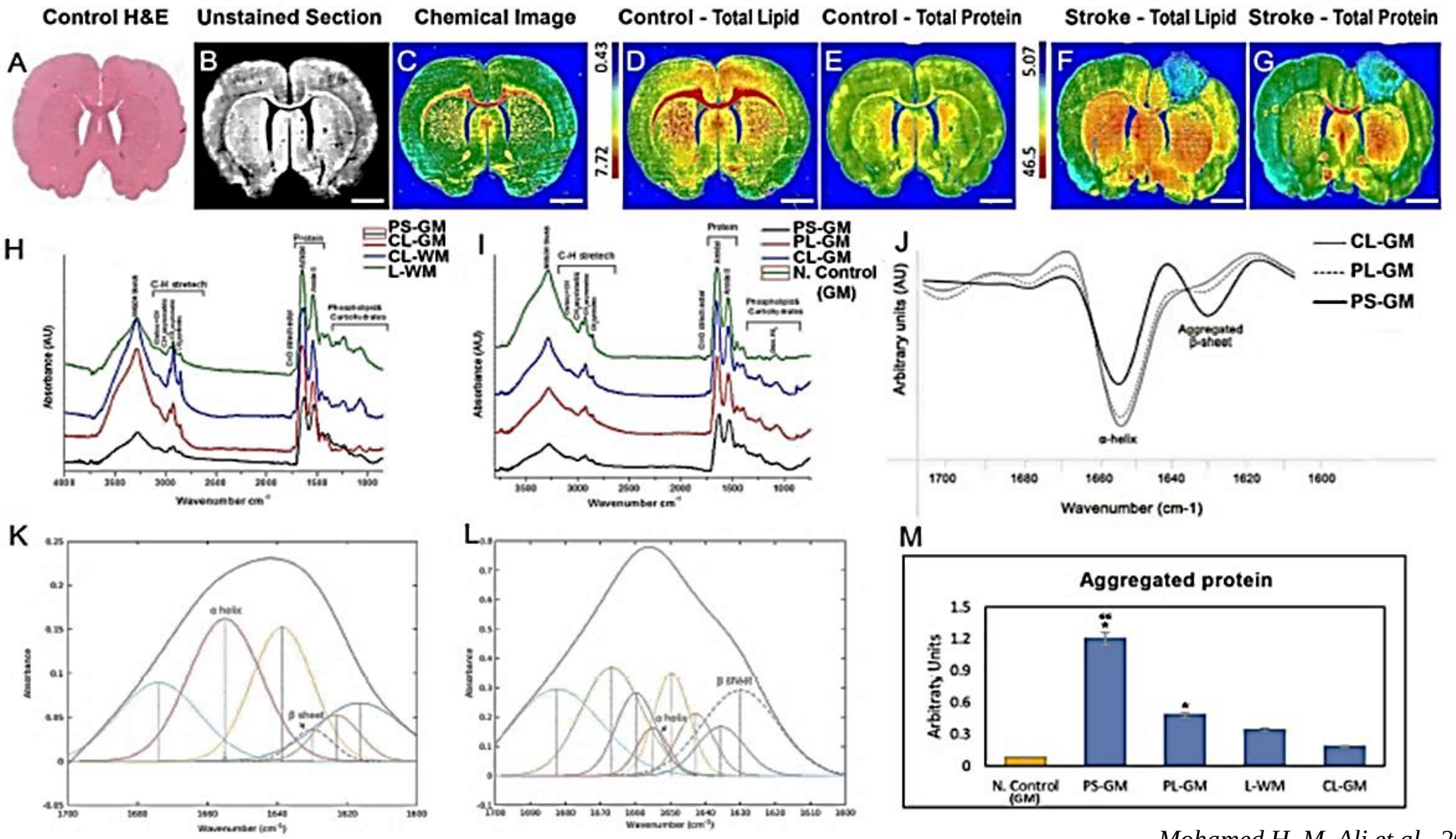

Mohamed H. M. Ali et al., 2018

FTIR, Raman and AFM characterization of the clinically valid biochemical parameters of the thrombi in acute ischemic stroke

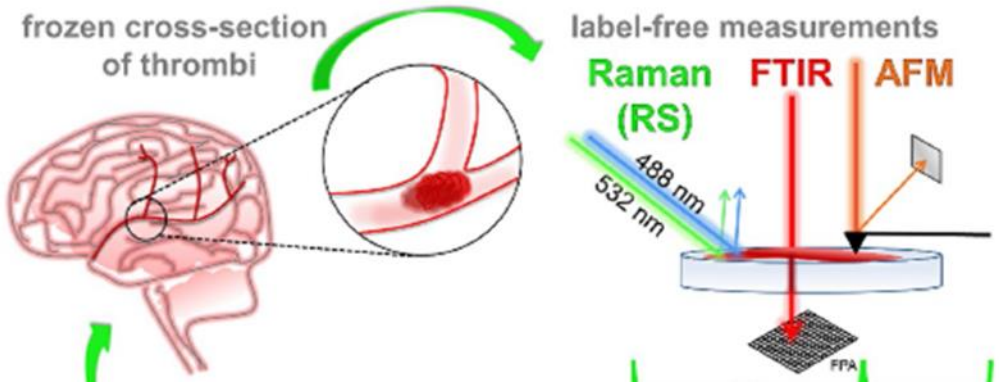

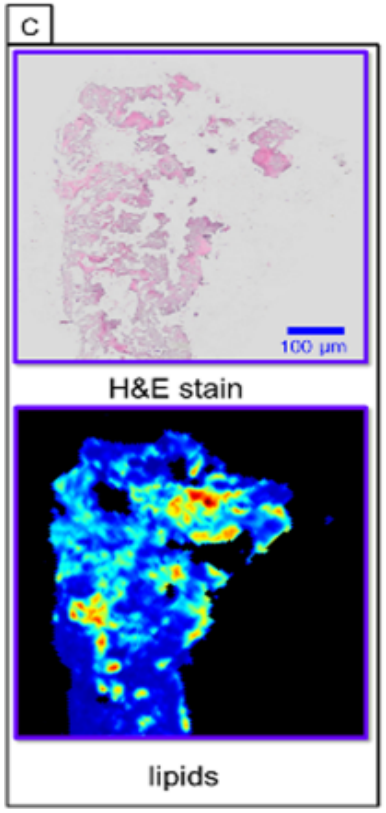

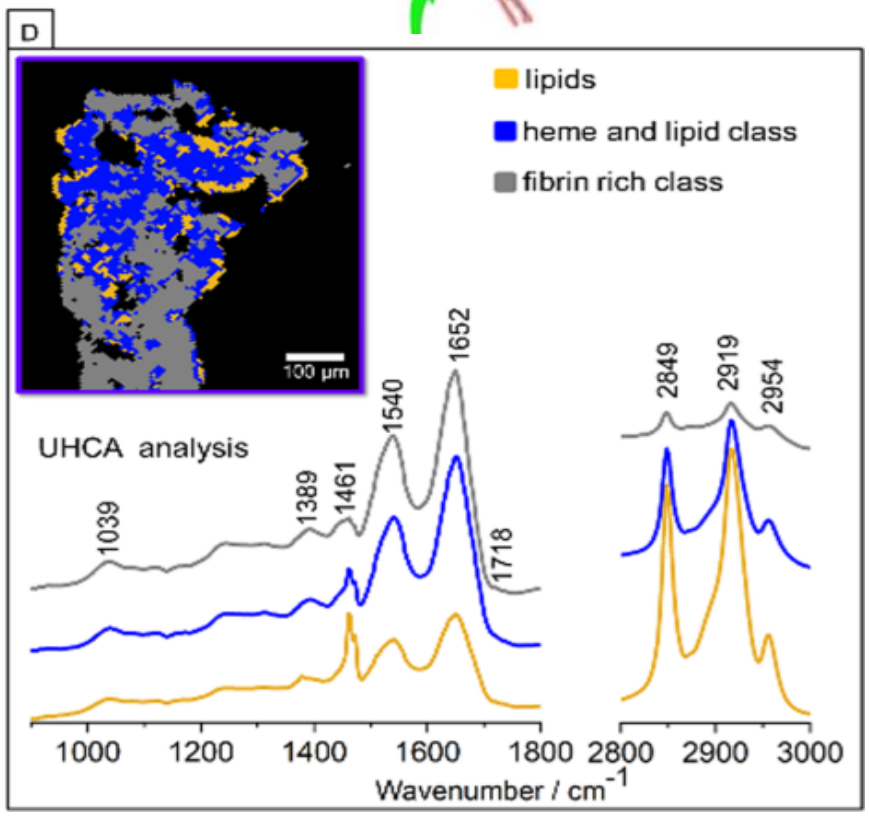

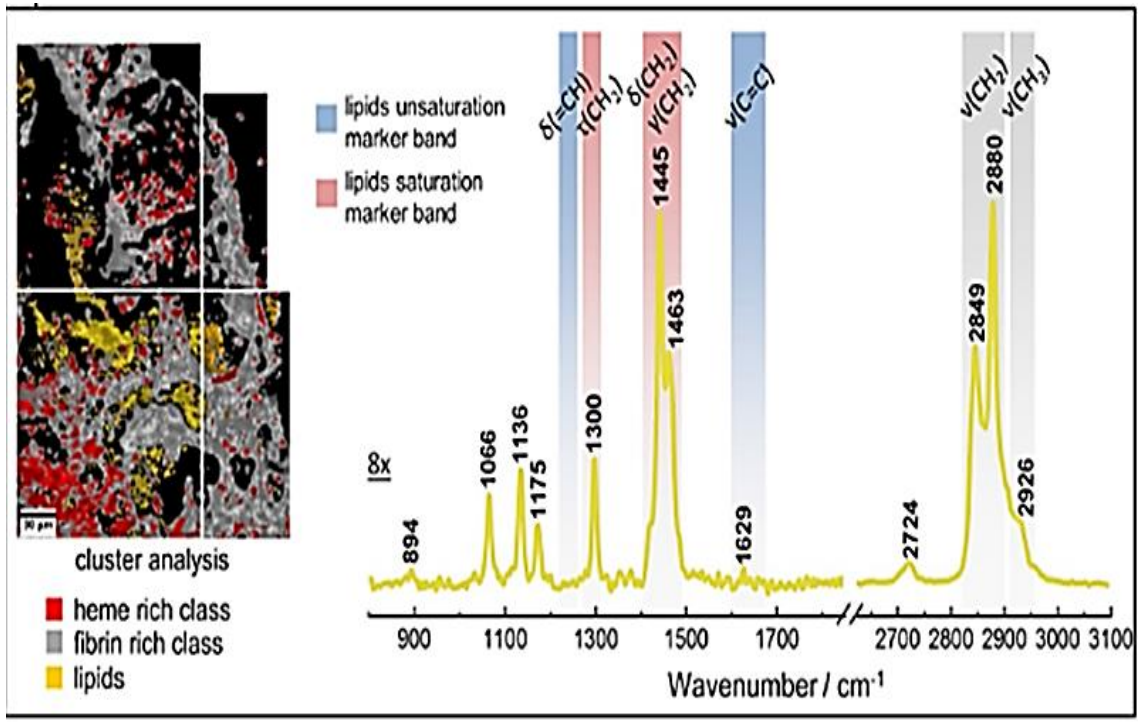

Blat et al., 2019

Synchrotron Radiation-Based FTIR Microspectroscopic Imaging of Traumatically Injured Mouse Brain Tissue Slices

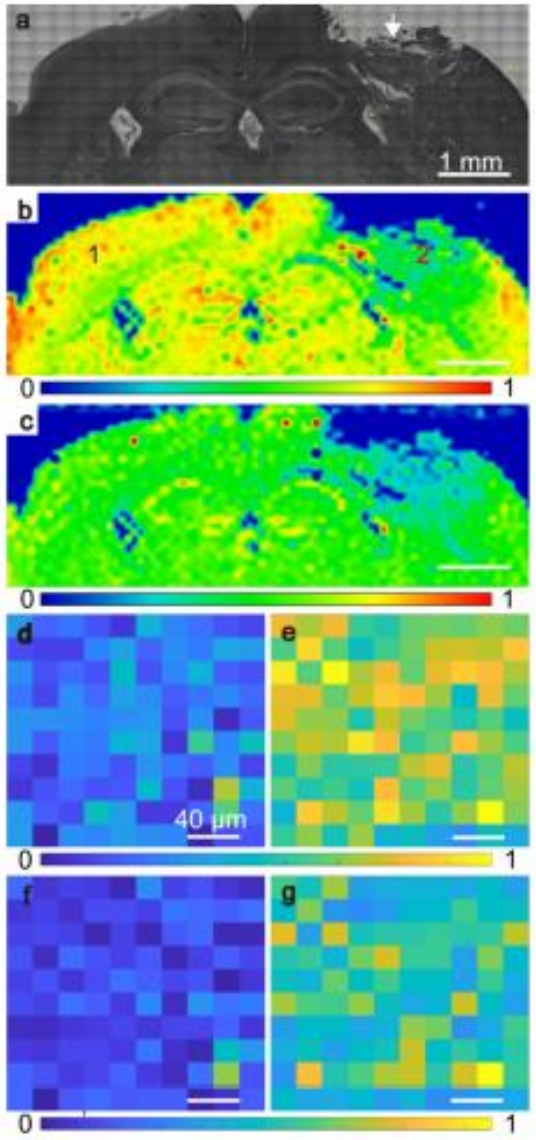

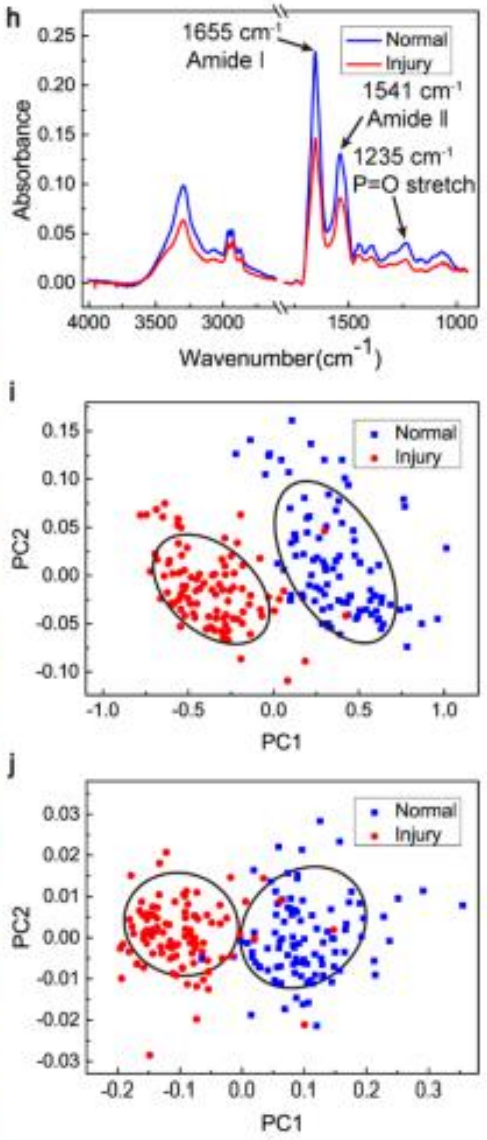

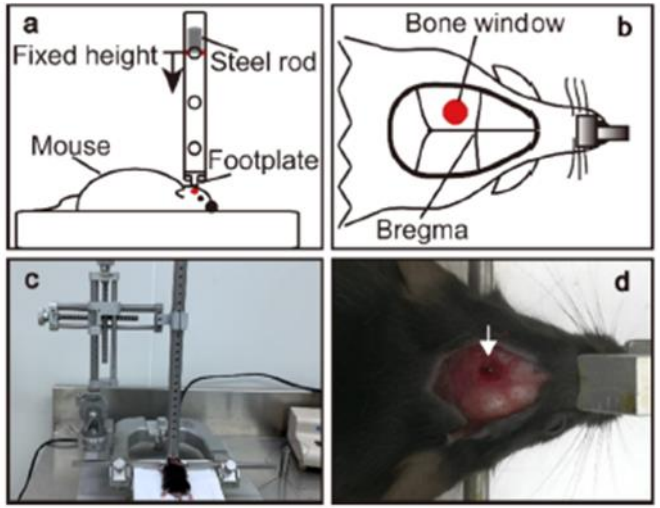

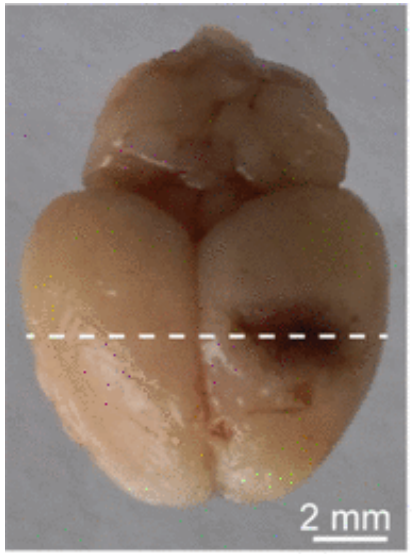

Visual image

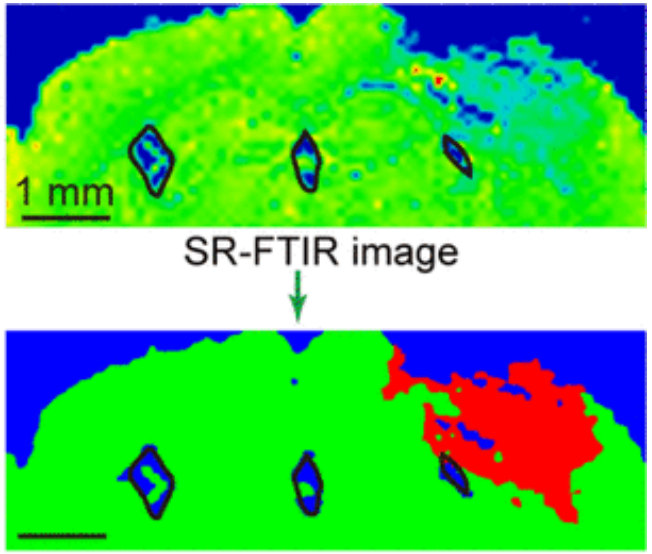

Guo et al., 2020

Label-free FTIR spectroscopy detects and visualizes the early stage of pulmonary micrometastasis seeded from breast carcinoma

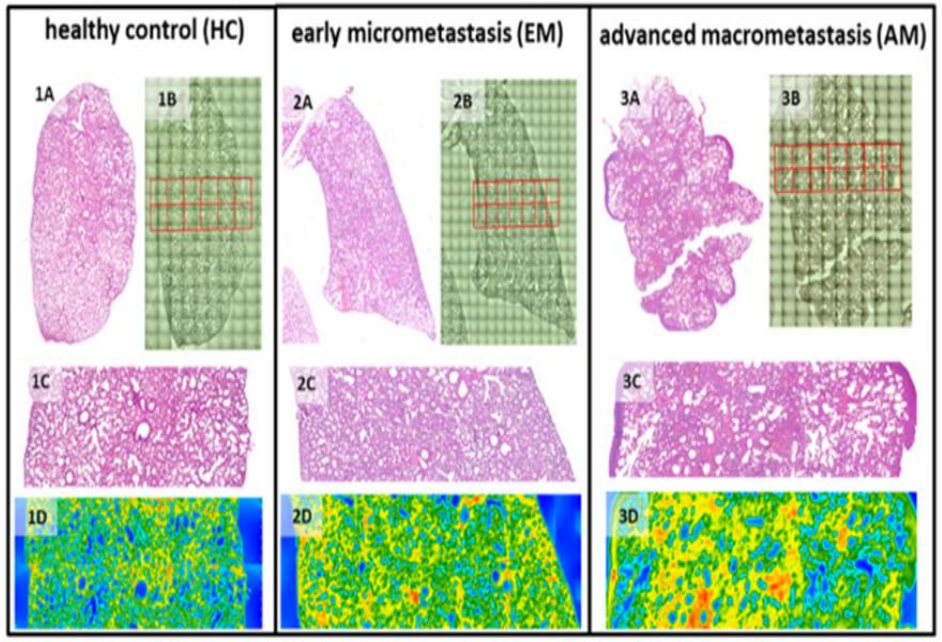

Fig. 2. FTIR spectroscopic imaging of lung cross-sections of control BALB/cAnNCrl mice and BALB/cAnNCrl mice three- (early micrometastasis, EM) and five (advanced macrometastasis, AM) after orthotopic inoculation with viable 4 T1 tumor cells: A. H&E stained cross-sections (magnification 20×), B. white light with marked regions of interest (ROI; magnification 15×), C. magnified H&E stained ROIs, and D. IR images for the protein distribution (amide I: 1702–1610 One red square corresponds to the area of 700 × 700 μm^2.

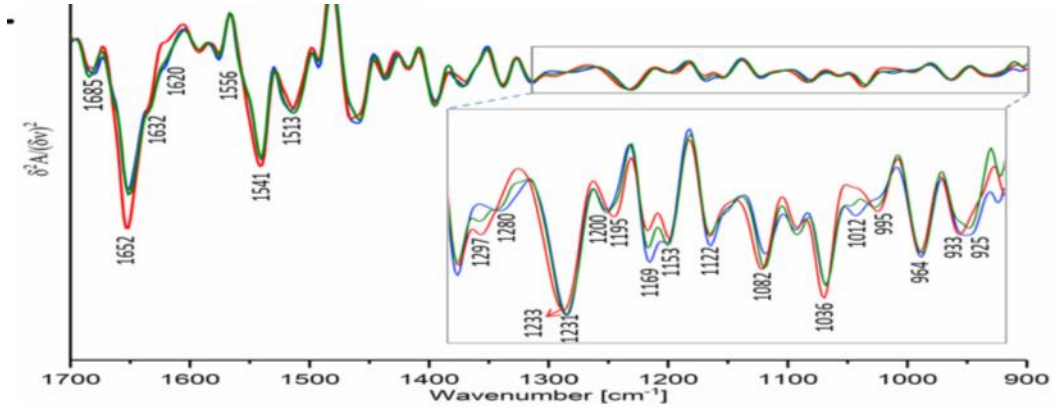

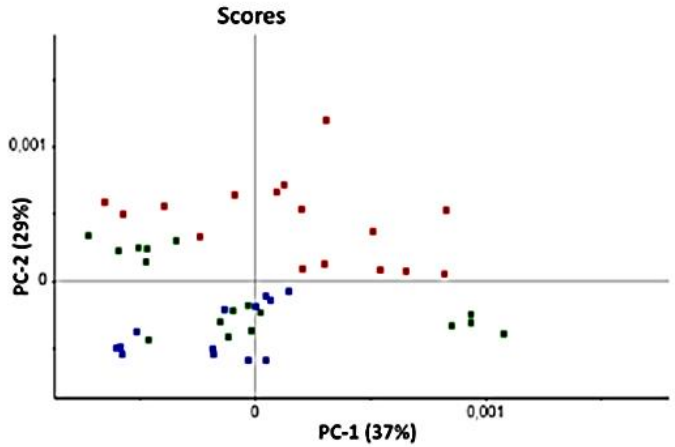

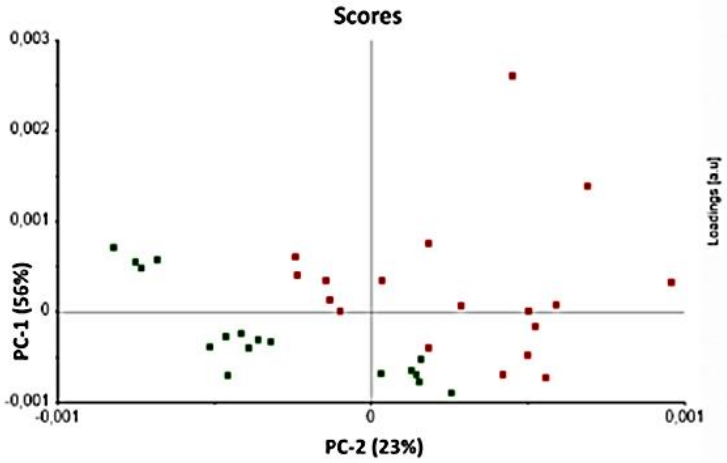

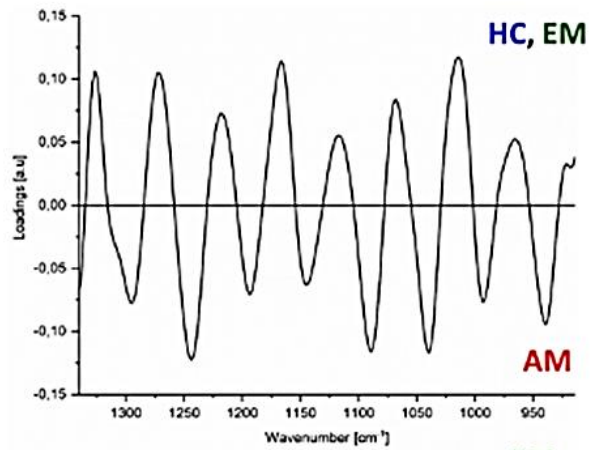

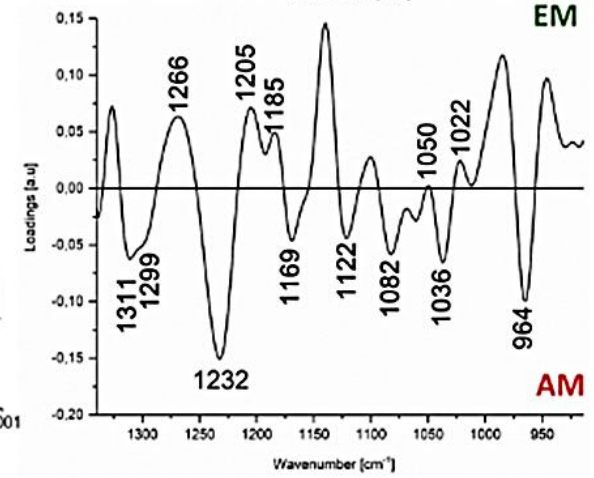

healthy control (HC) early micrometastasis (EM) advanced macrometastasis (AM)

Chrabaszcz et al., 2018

FPA-FTIR Microspectroscopy for Monitoring Chemotherapy Efficacy in Triple-Negative Breast Cancer

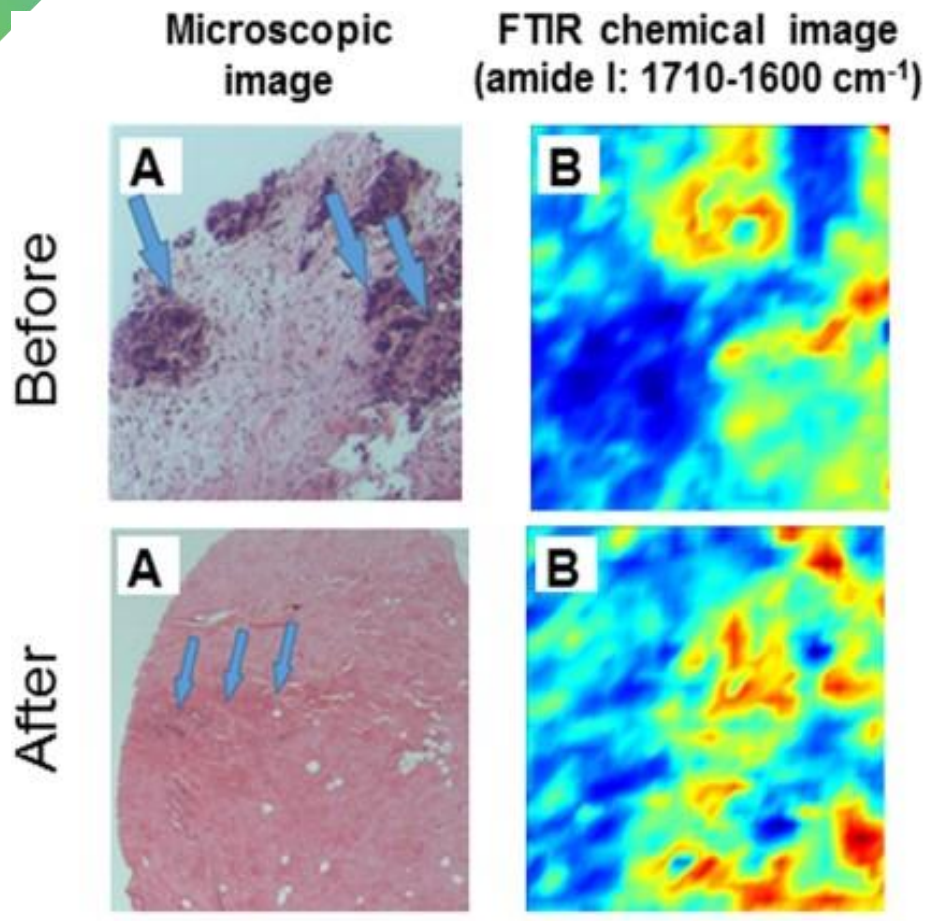

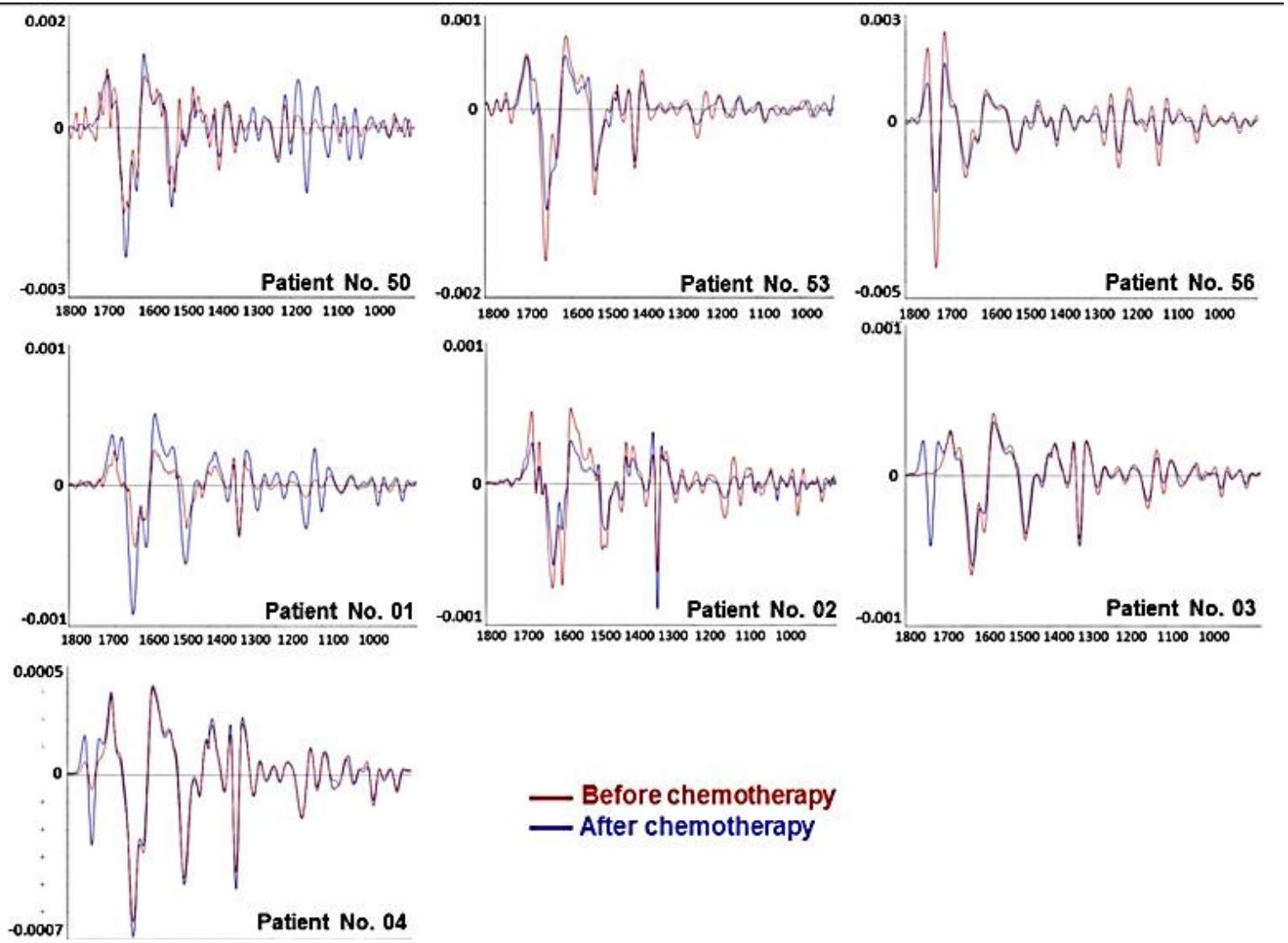

Zawlik et al., 2016

Challenges in Biology and Medicine with Synchrotron Infrared Light

P. Dumas[a], L.M. Miller[b] and M.J. Tobin[c]
[a]SOLEIL Synchrotron, Saint-Aubin, BP 48, 91192 Gif-sur-Yvette Cedex, France

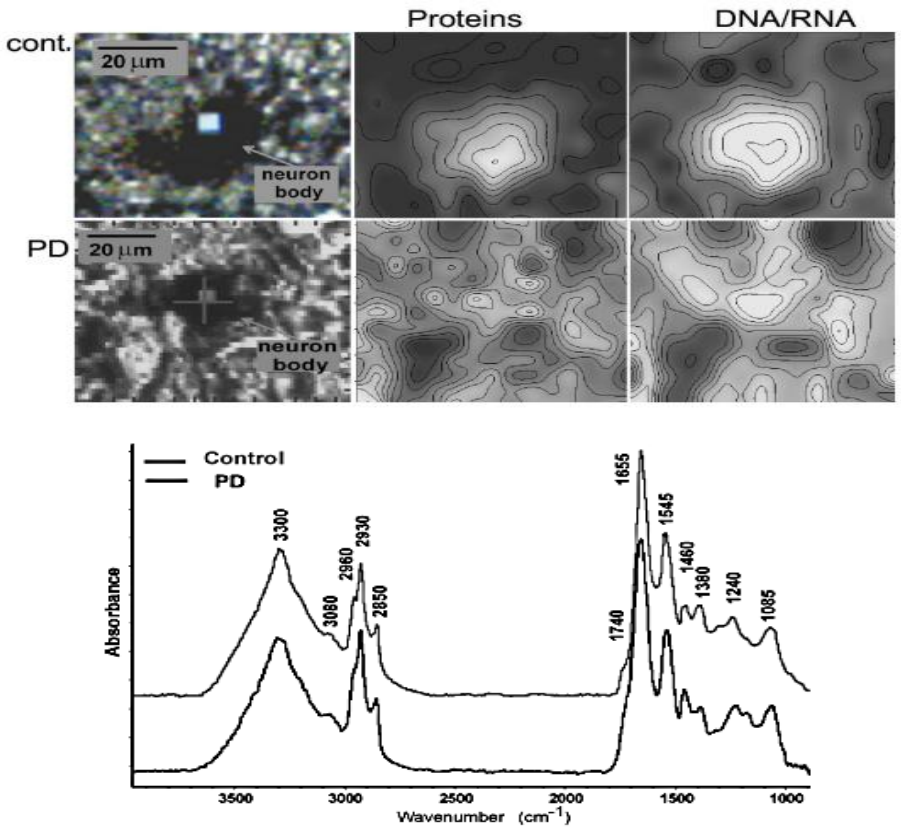

Fig. 12. The comparison of FTIR absorption spectra acquired in the neurons of substantia nigra for the control and Parkinson's diseased (PD) cases. Spectra were collected with a $6 \times 6\ \mu m^2$ aperture.

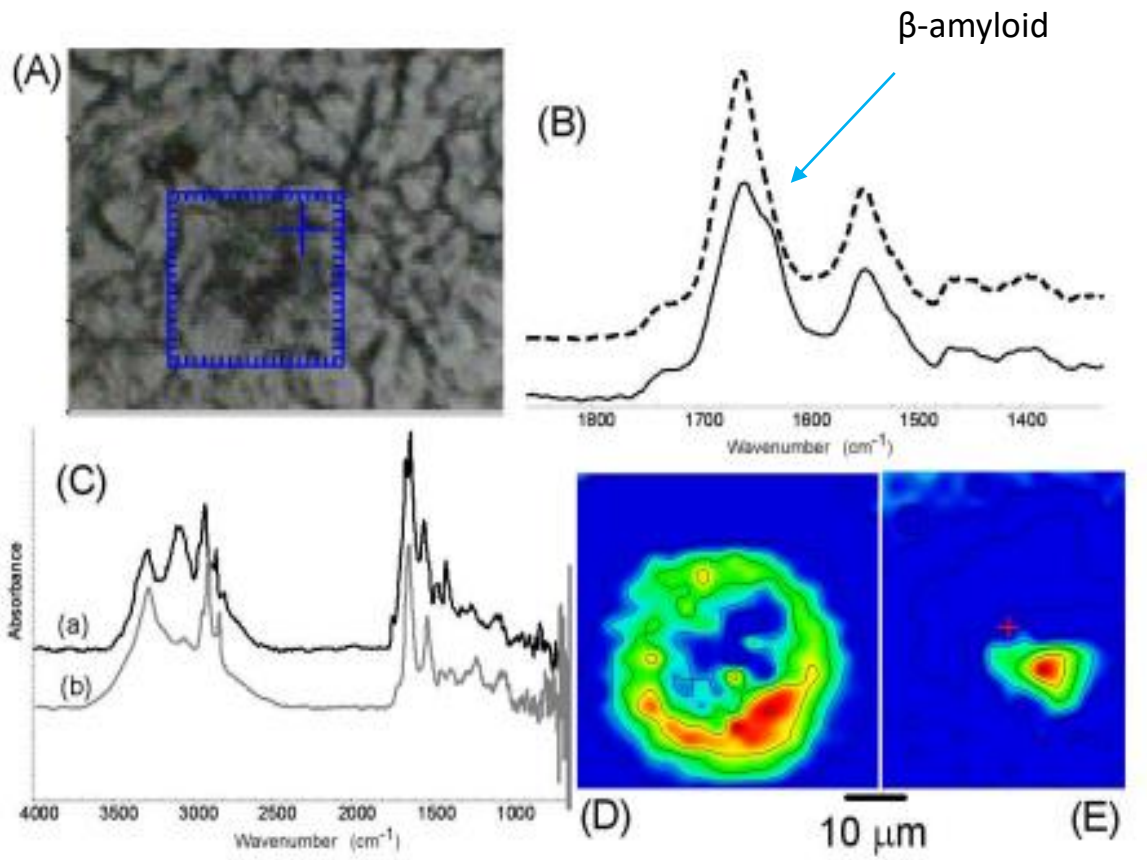

(A) Light microscope image of Alzheimer's diseased brain tissue. (B) Infrared spectra recorded inside and outside the plaque, showing the shoulder at 1630 cm^{-1}, assigned to β-amyloid. (C) Infrared spectra from inside the plaque. One of them displays additional absorption features, which are assigned to creatine. (D) Infrared image of amyloid plaque distribution, calculated as a peak height ratio of 1630/1655 cm−1 . (E) Chemical image of creatine distribution inside the plaque.

Structural determination of protein-based polymer blends with a promising tool: combination of FTIR and STXM spectroscopic imaging

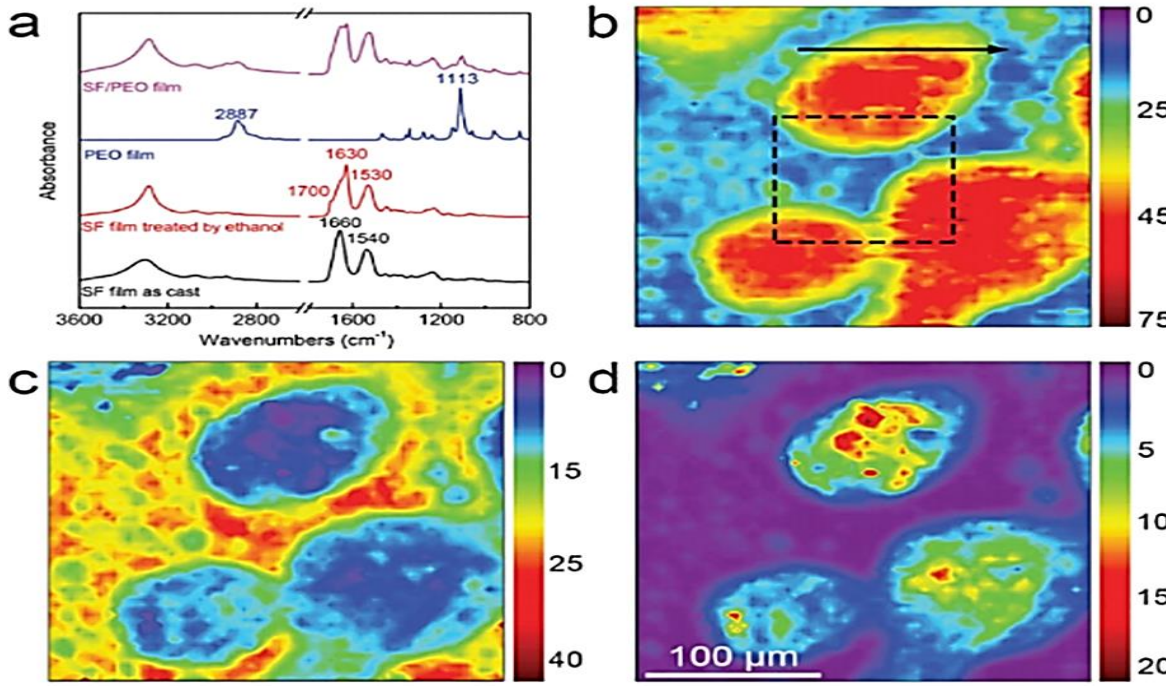

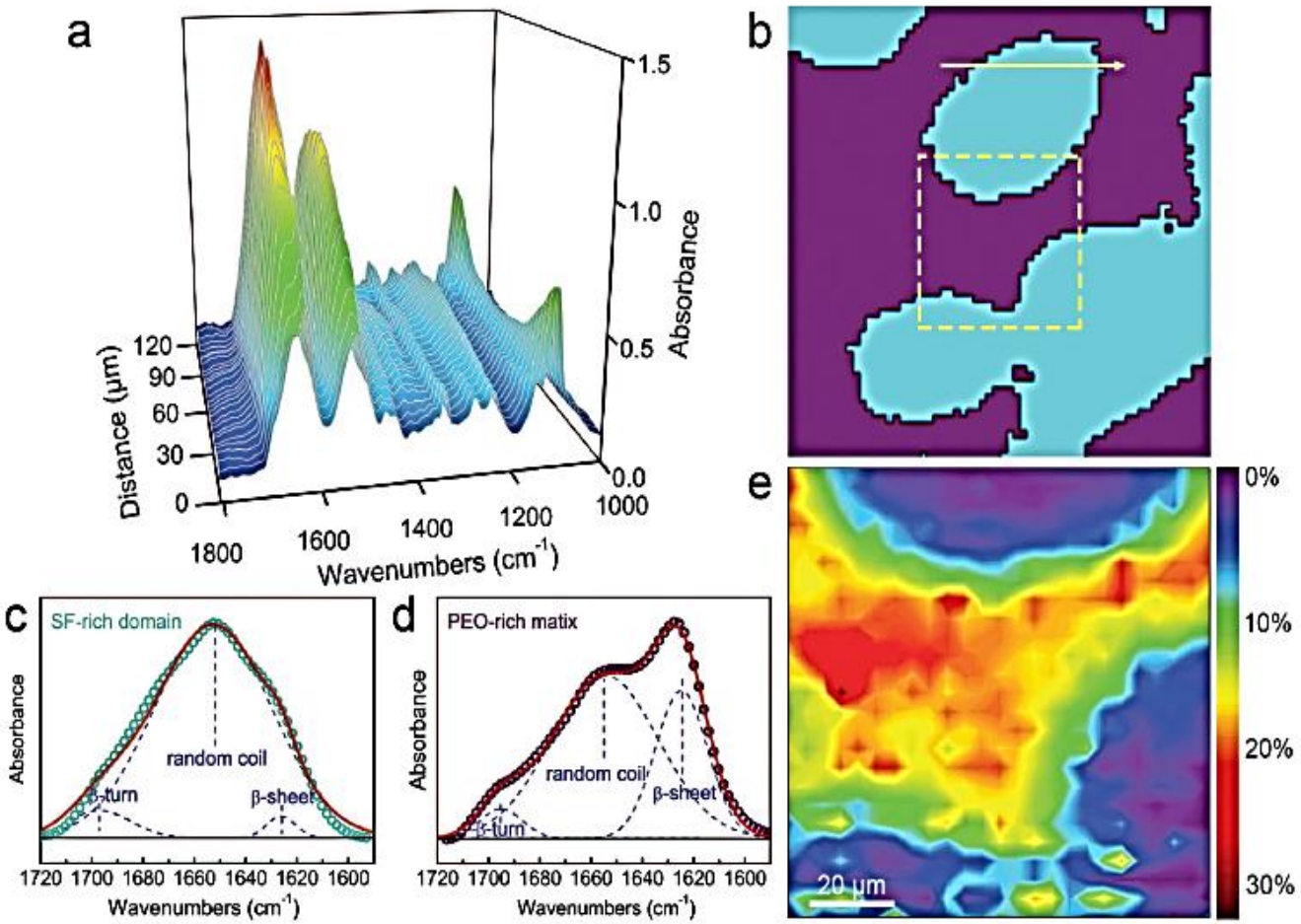

FTIR spectra and FTIR images of the SF/PEO blend. (a) FTIR spectra of SF film as a cast, SF film treated with 70% ethanol solution, pristine PEO film, and SF/PEO blend film; (b) SF-specific FTIR image of the SF/PEO blend; (c) PEO-specific image of the SF/PEO blend; (d) ASF/APEO image of the SF/PEO blend. The scale bars in (b), (c), and (d) are the same.

Ling et al., 2014

WAXS characterization of Scaffold

Fourier Transform Infrared Spectroscopy

Table 1. The structural conformation ratios in gelatin, silk fibroin, and silk fibroin-gelatin scaffolds derived from deconvoluted amide I FTIR spectra.

Samples	Conformation content of samples [a]			
	β-sheet	Random coil	α-helix	β-turns
Gelatin	32.96 ± 1.0	34.12 ± 0.5	17.72 ± 0.7	17.20 ± 0.3
Silk fibroin	31.00 ± 1.2	32.69 ± 1.2	19.89 ± 1.5	16.41 ± 1.4
Scaffold 8:2	24.88 ± 0.5	36.58 ± 0.6	21.61 ± 1.2	23.54 ± 0.6
Scaffold 7:3	27.75 ± 1.6	29.47 ± 2.1	21.39 ± 0.5	23.38 ± 1.0

[a] Values are average ± standard derivation (N=3)

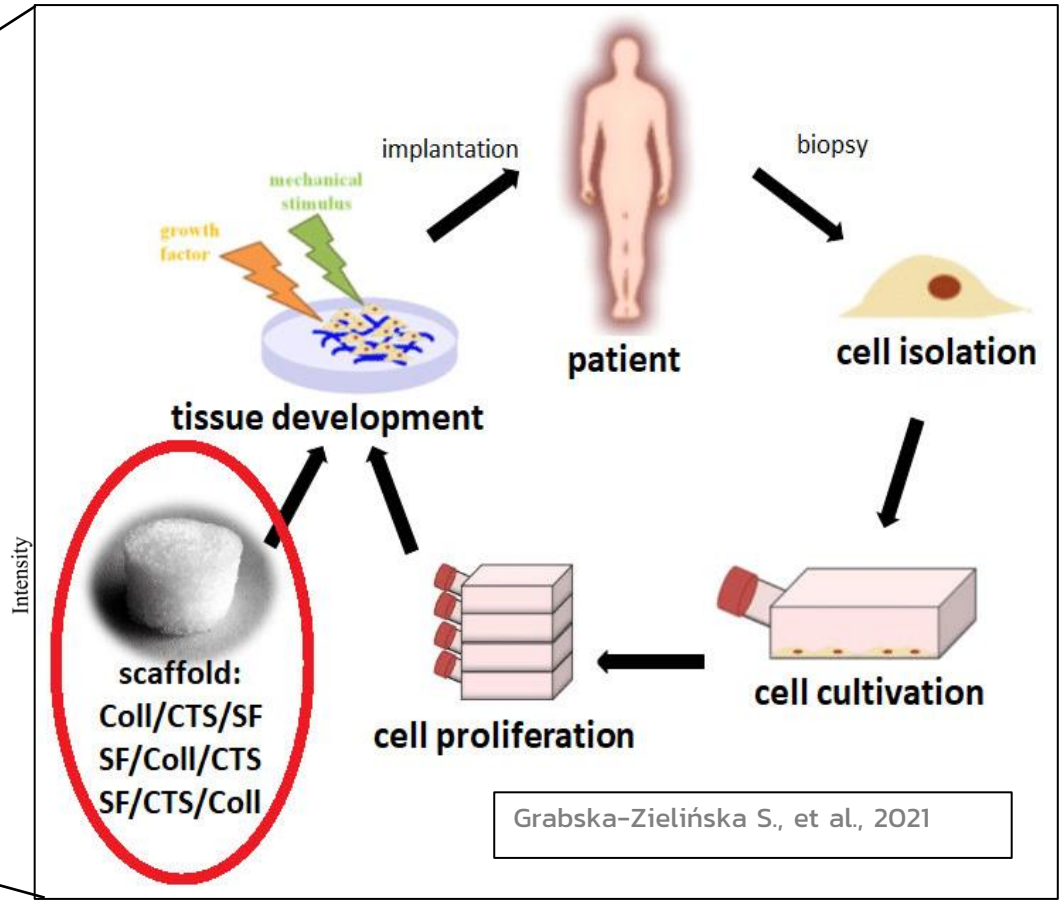

Wide-angle synchrotron X-ray scattering at BL 1.3W

Naksuwan K. et al., 2023

THAI SYNCHROTRON NATIONAL LAB

Siam Photon

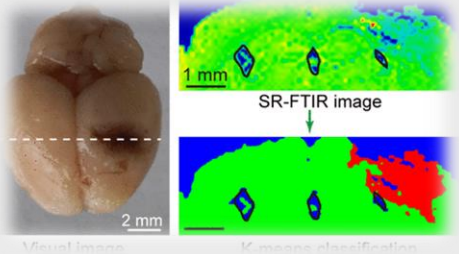

Diagnosis of diseases

Drug development

Applications of synchrotron FTIR techniques in medical fields

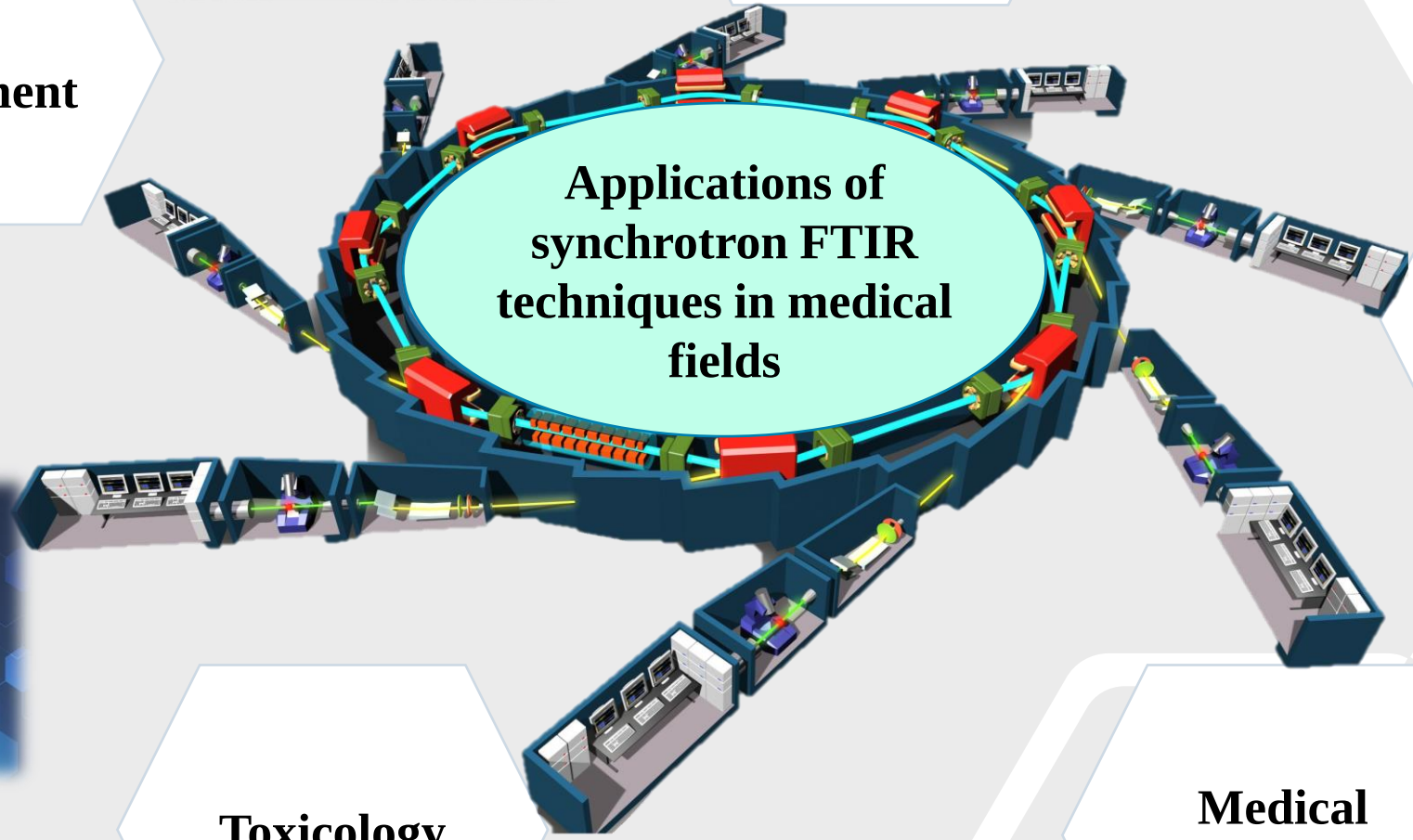

Analysis of biomolecules

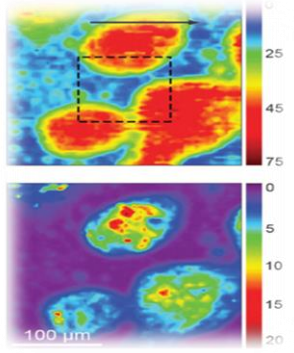

Toxicology

Medical imaging


THANK YOU
Siam Photon
THAI
SYNCHROTRON
NATIONAL LAB

SR-FTIR as a tool for quantitative mapping of the content and distribution of extracellular matrix in decellularized book-shape bioscaffolds

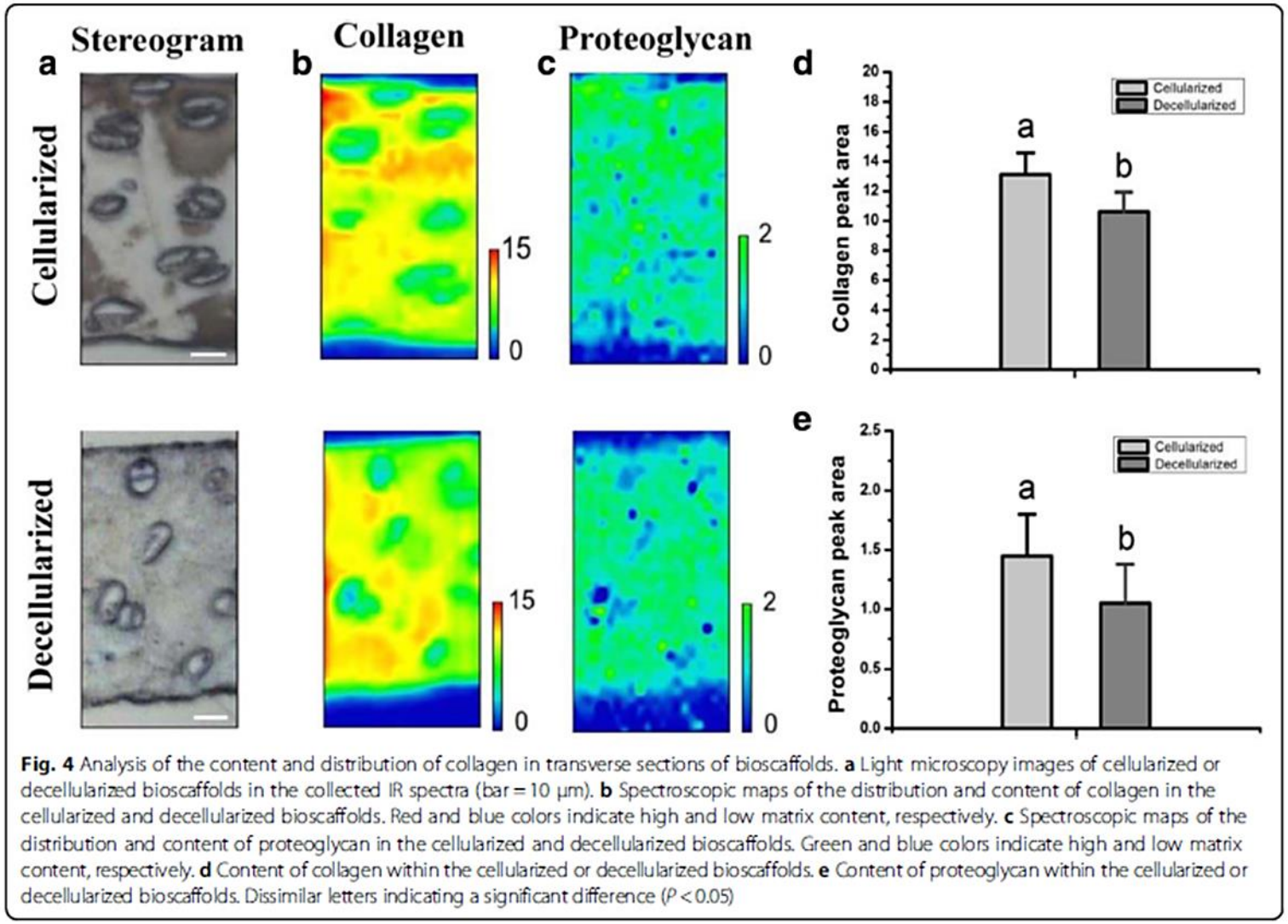

Fig. 4 Analysis of the content and distribution of collagen in transverse sections of bioscaffolds. **a** Light microscopy images of cellularized or decellularized bioscaffolds in the collected IR spectra (bar = 10 μm). **b** Spectroscopic maps of the distribution and content of collagen in the cellularized and decellularized bioscaffolds. Red and blue colors indicate high and low matrix content, respectively. **c** Spectroscopic maps of the distribution and content of proteoglycan in the cellularized and decellularized bioscaffolds. Green and blue colors indicate high and low matrix content, respectively. **d** Content of collagen within the cellularized or decellularized bioscaffolds. **e** Content of proteoglycan within the cellularized or decellularized bioscaffolds. Dissimilar letters indicating a significant difference ($P < 0.05$)

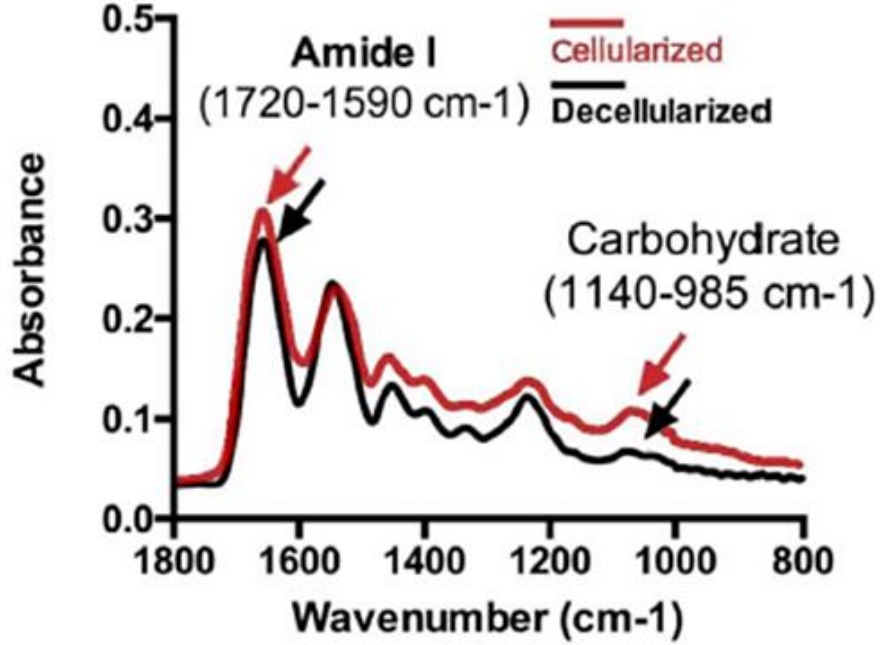

Fig. 3 Representative infrared spectra: Red color line indicates cellularized bioscaffolds; Black color line indicates decellularized bioscaffolds. Note: Peaks of amide I and carbohydrate were indicative for collagen and proteoglycan, respectively

Zhou et al., 2018

International Journal of Molecular Sciences

MDPI

Article

Evaluation of Melanoma (SK-MEL-2) Cell Growth between Three-Dimensional (3D) and Two-Dimensional (2D) Cell Cultures with Fourier Transform Infrared (FTIR) Microspectroscopy

Tarapong Srisongkram [1], Natthida Weerapreeyakul [2,3,*] and Kanjana Thumanu [4]

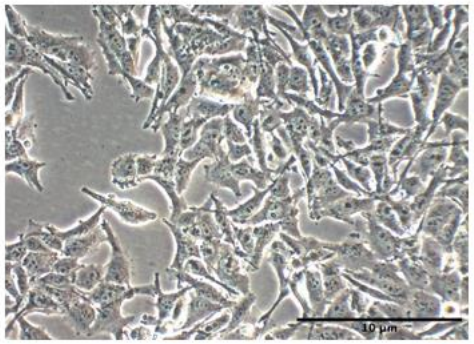

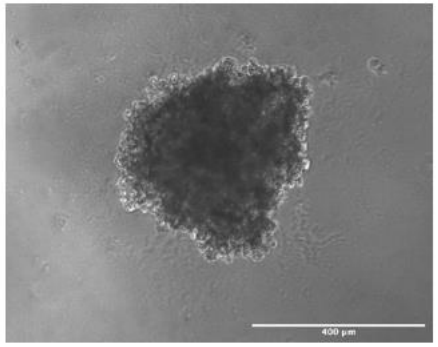

FTIR data represent the characteristic differences between the 2D cell culture and 3D spheroids and their respective ability to distinguish variations in the 3D spheroids.

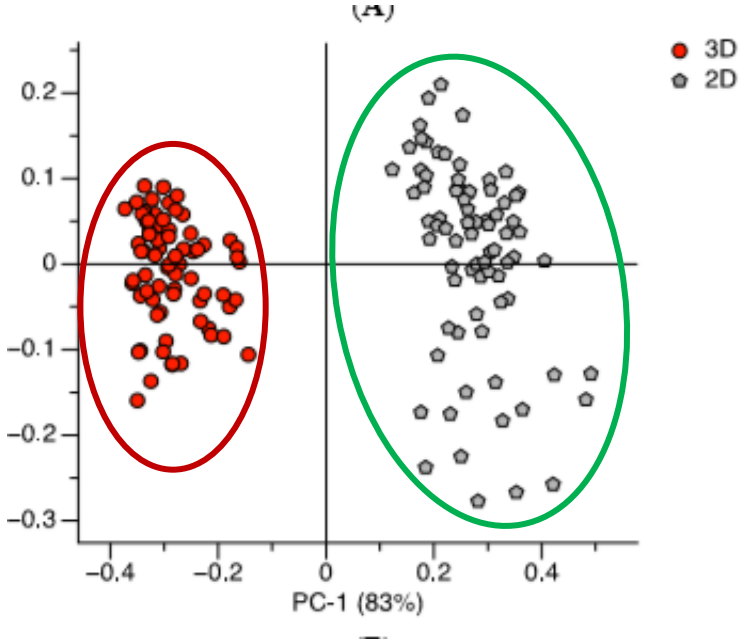

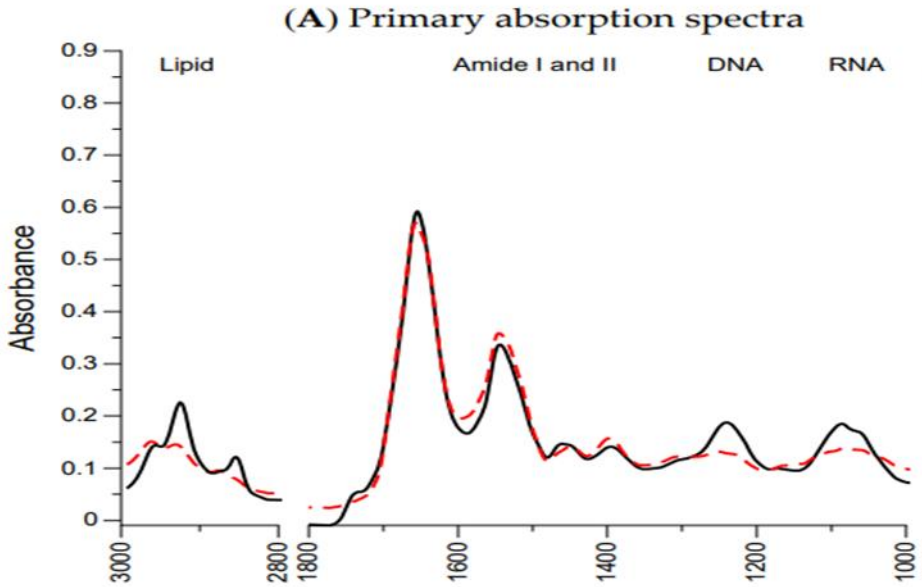

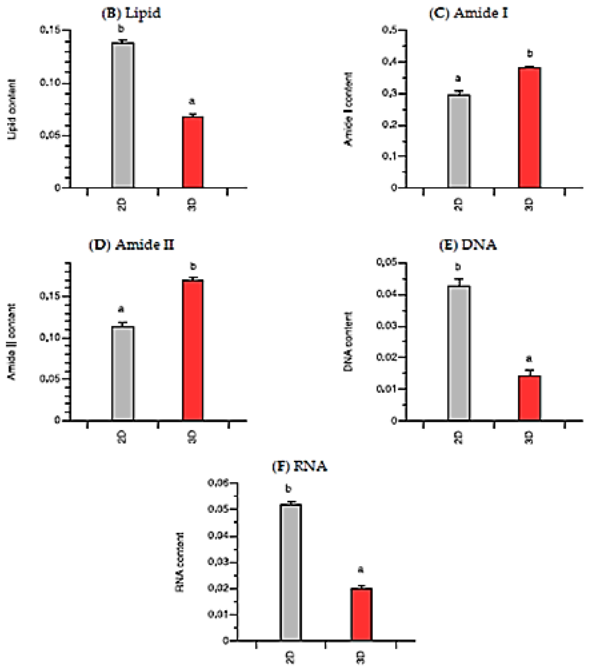

Fourier transform infrared spectroscopy

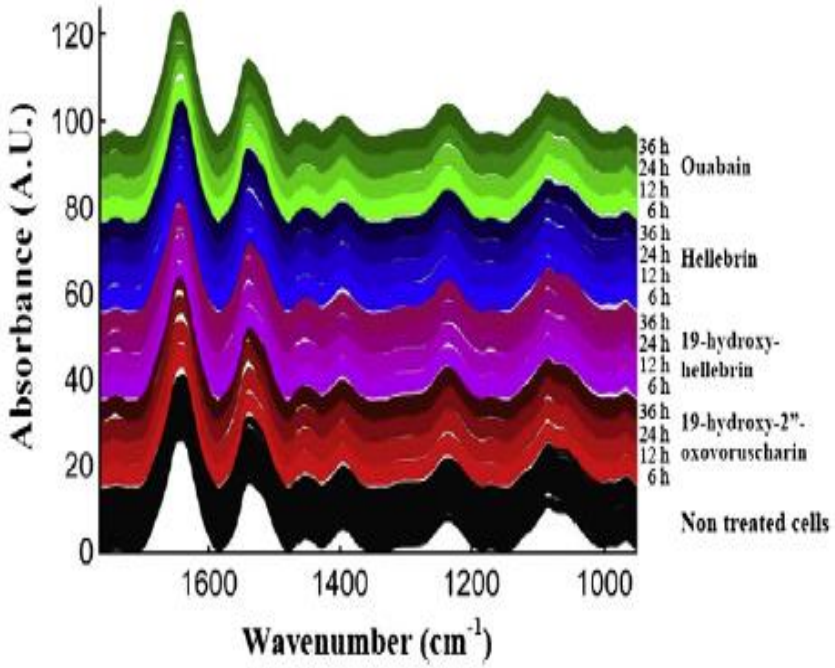

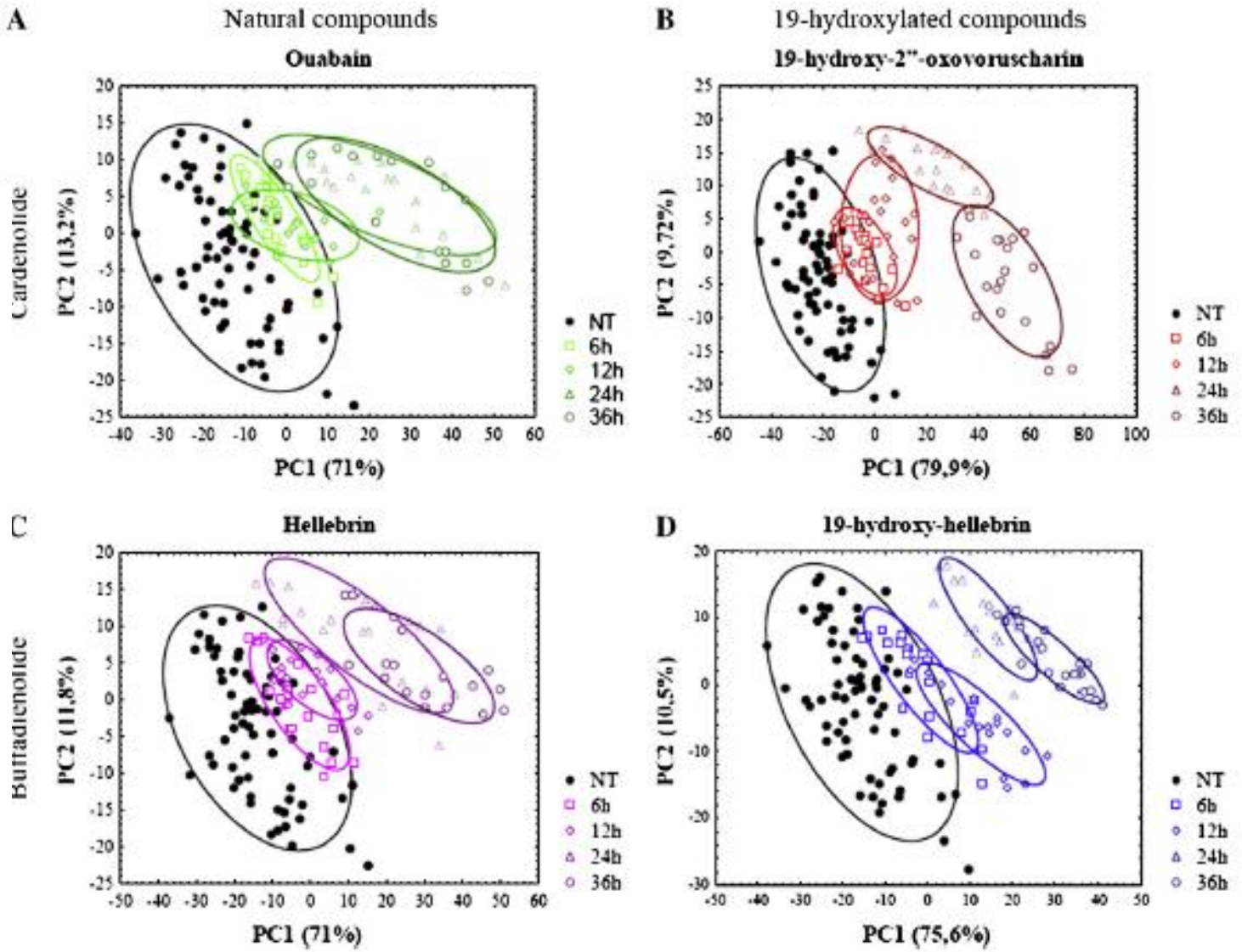

Fig. 3. PCA scores on PC1 and PC2 computed for each drug including all exposure times. A: Ouabain, B: 19-hydroxy-2"-oxovoruscharin, C: Hellebrin, D: 19-hydroxy-hellebrin. Projections of untreated cells recorded for each incubation time were drawn in black filled circles. Squares: 6 h exposure to CS, diamond, 12 h; triangle, 24 h; empty circles, 36 h. The percentage of variance in the data explained by each PC is reported in brackets. 95% confidence ellipses are reported.

Gasper et al., 2010

Label-free FTIR spectroscopy detects and visualizes the early stage of pulmonary micrometastasis seeded from breast carcinoma

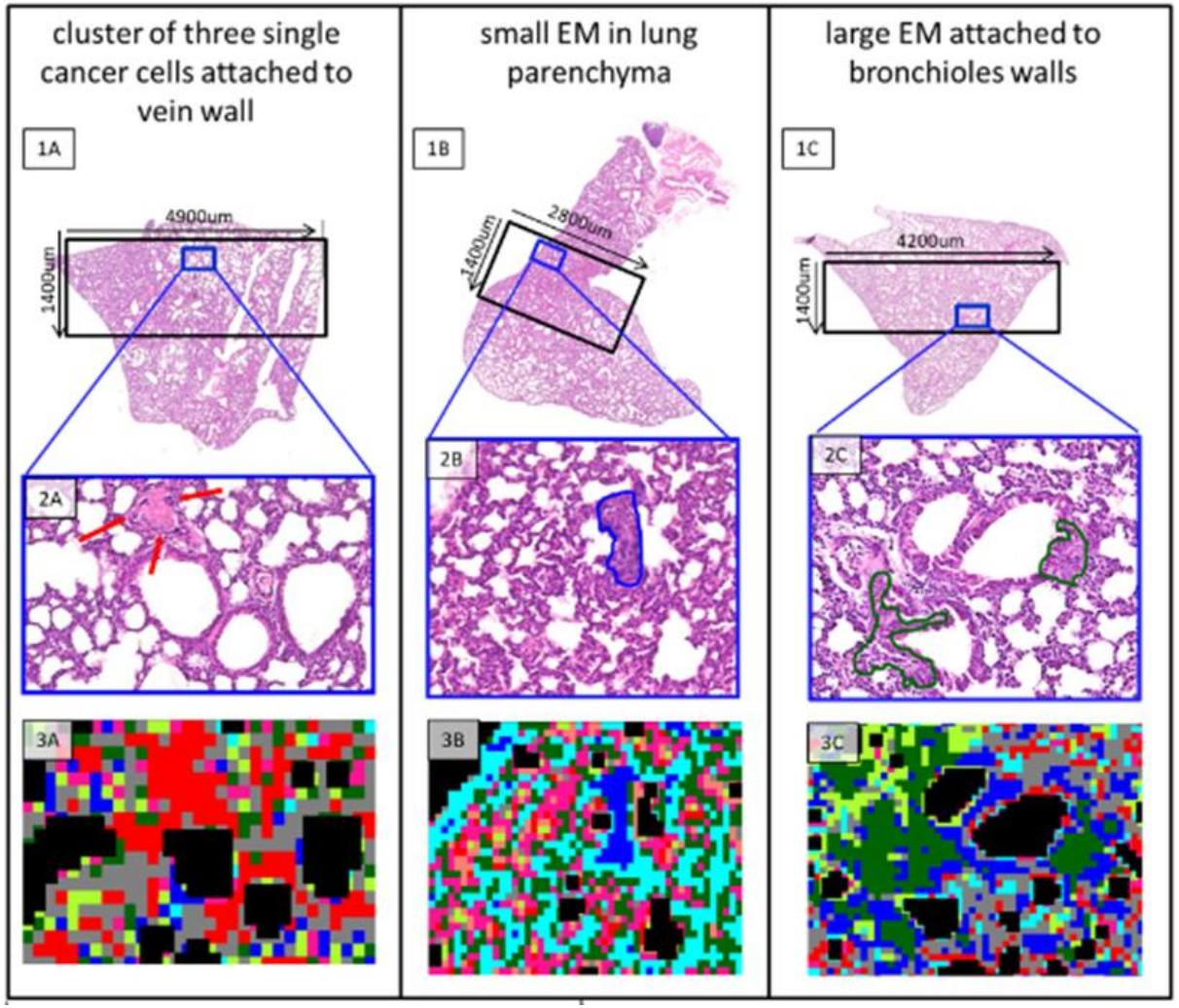

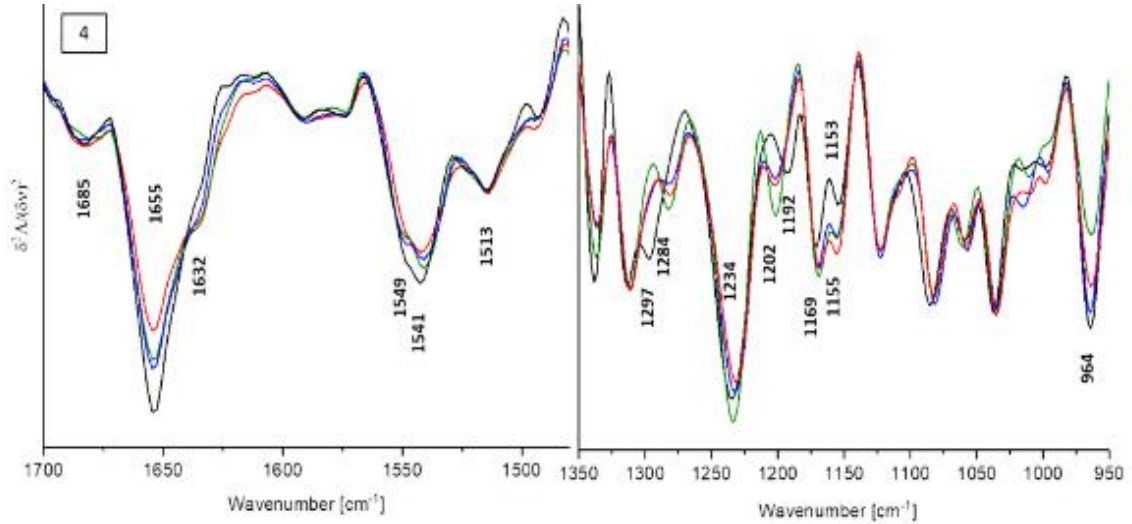

Fig. 6. 1A–C. H&E stains of the whole lung cross sections from the early metastatic phase with marked ROIs (in black) and localization of micrometastasis (in blue). 2. Enlarged H&E stains showing cancer cells: ca. 123 μm^2 in blood clot: ca. 4703 μm^2 (A) micrometastic sites surrounded by inflammatory cells: ca. 4717μm^2 (B) and in bronchioles edges left: ca. 3047 μm^2 and right: ca.6516 μm^2 (C). 3. UHCA false-color maps and (4) their mean second derivative FTIR spectra extracted from classes with micrometastases (red, blue and green from 3A, B and C, respectively) and compared with the spectrum of tumor from the AM phase (black trace, cf. *Fig. 5.3B)*. (For interpretation of the references to color in this figure legend, the reader is referred to the web version of this article.)

Chrabaszcz et al., 2018

Determination of physicochemical properties of delipidized hair

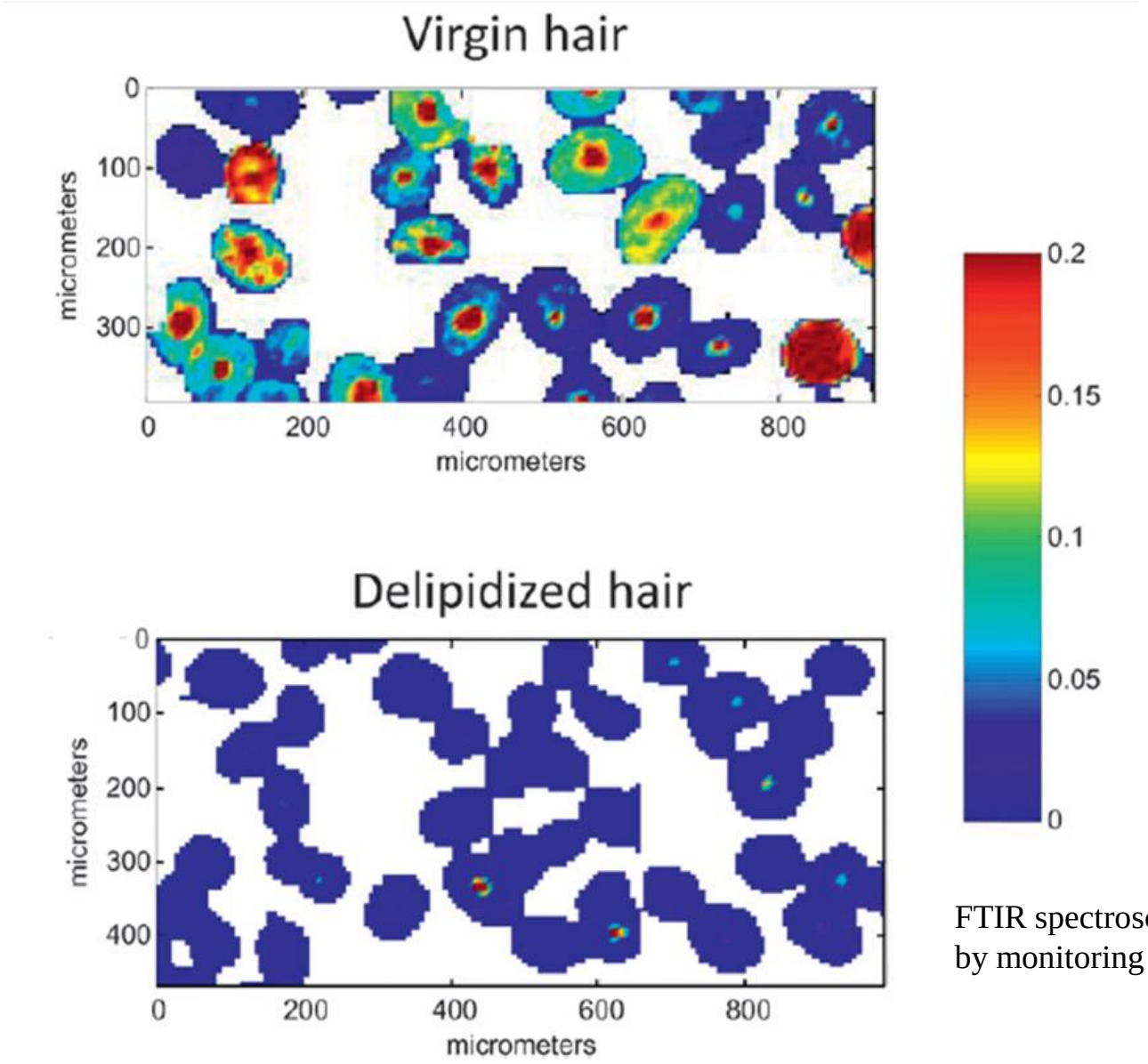

FTIR spectroscopic imaging of hair cross sections obtained by monitoring the lipid peak (2850 cm^{-1}).

Single Cell Imaging of Nuclear Architecture Changes

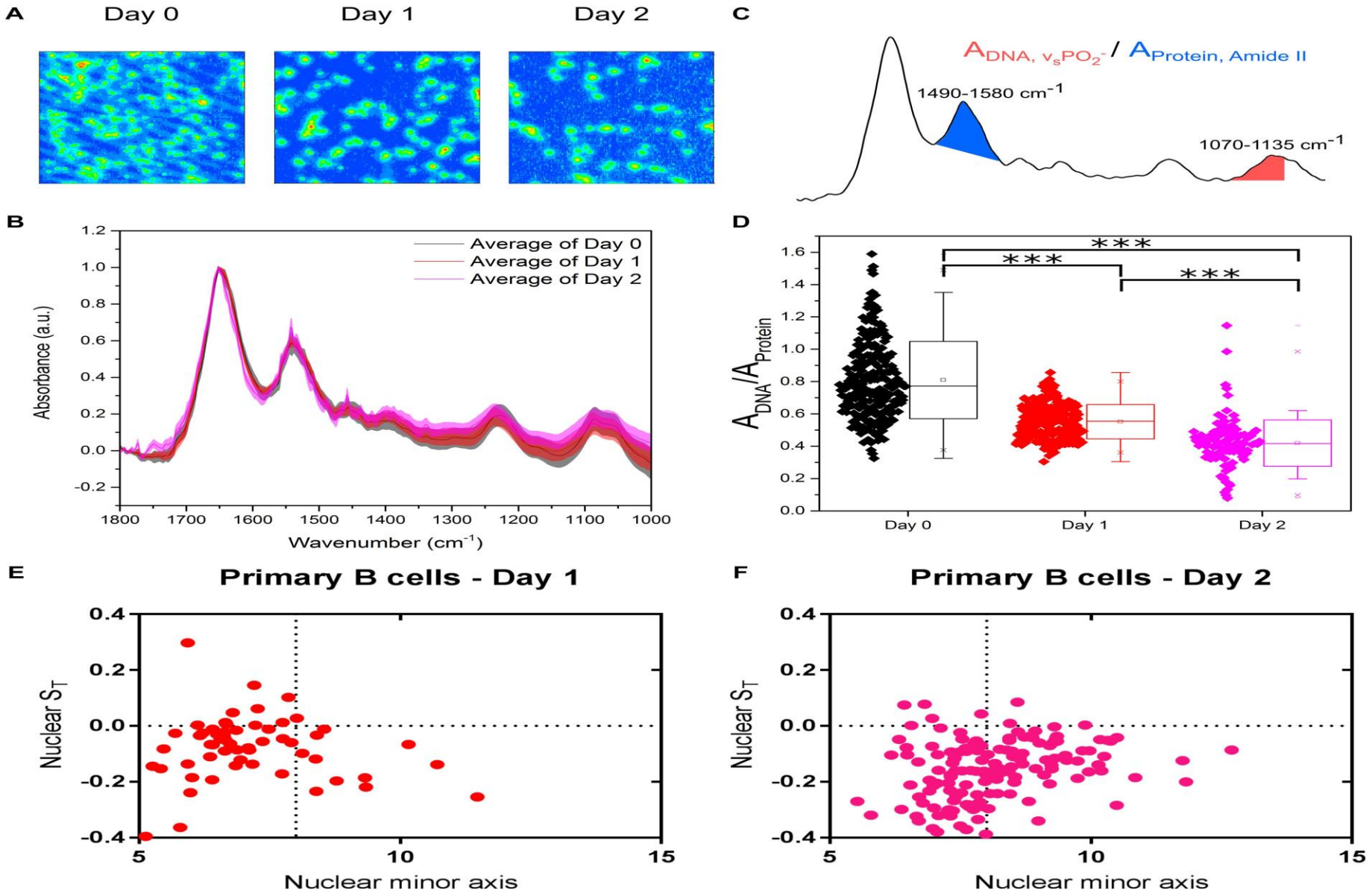

Brandstrup Morrish et, al., 2019